

Galaxy Evolution in the $z=0.4274$ Cluster MS1621.5+2640¹

Simon L. Morris and J. B. Hutchings

Dominion Astrophysical Observatory, National Research Council,
5071 West Saanich Road, Victoria, B.C., V8X 4M6, Canada,
e-mail: Simon.Morris@hia.nrc.ca, John.Hutchings@hia.nrc.ca

R. G. Carlberg and H. K. C. Yee

Department of Astronomy, University of Toronto, Toronto,
Ontario M5S 1A7, Canada,
email: carlberg@moonray.astro.utoronto.ca, hyee@makalu.astro.utoronto.ca

Erica Ellingson

CASA, University of Colorado, Boulder, CO 80309-0389,
email: e.elling@pisco.colorado.edu

Mike L. Balogh

Department of Physics and Astronomy, University of Victoria,
Victoria, B.C., V8W 3P6, Canada,
email: Balogh@uvphys.phys.uvic.ca

R. G. Abraham

Institute of Astronomy, University of Cambridge, Madingley Rd.,
Cambridge CB3 0HA, UK,
email: abraham@ast.cam.ac.uk

and

Tammy A. Smecker-Hane

Department of Physics and Astronomy, University of California, Irvine, CA 92797-4575,
email: smecker@carina.ps.uci.edu

ABSTRACT

We discuss the galaxy population of the rich cluster MS1621.5+2640 at $z=0.4274$, based on spectra and imaging in a field of size 9 arcmin by 23 arcmin

¹Based on Observations taken at the Canada-France-Hawaii Telescope, which is operated by the NRC of Canada, CNRS of France and the University of Hawaii.

(~ 2 by $5 h^{-1}$ Mpc). The sample comprises 277 galaxies, of which 112 are cluster members, 7 are ‘near-members’, and 47 are field galaxies in the redshift range $0.37 \leq z \leq 0.50$. The results are analyzed and compared with the $z=0.2279$ rich cluster Abell 2390. MS1621.5+2640 has a higher blue fraction, a younger stellar population, and is a less evolved cluster. We do not find strong evidence of significant excess star formation compared with the field, although there is a small population of outlying near-members that is unusually blue and that may be affected by the cluster. There is a substantial population of red galaxies with significant $H\delta$ absorption, which are not easily explained by any simple form of modeled star formation history. We detect two distinct populations of cluster galaxies: those where star formation ceased some time ago, and those with a gradual decrease over many Gyr. Our data suggests that the cluster formed by accretion from the field, with truncation of the star formation beginning at very large radii (>2 times the virial radius). The truncation process does not seem to be a sharp one though, in that lower-luminosity early-type galaxies in the inner core of the cluster are seen with significant $H\delta$ absorption, indicating some star formation within the last 1-2 Gyr. Some combination of stripping of gas from the outer parts of the galaxy, together with gradual exhaustion of the gas in the inner parts would be consistent with our data.

Subject headings: galaxies: clusters: individual (MS1621.5+2640) – galaxies: distances and redshifts – galaxies: photometry – galaxies: stellar content

1. Introduction

Clusters at intermediate redshift allow us to study evolutionary processes in cluster structure, cluster growth by infall, and the evolution of cluster galaxies themselves, in morphology and stellar populations. Study of a well selected set of clusters at different redshifts provide snapshots of these processes at different epochs. The Canadian Network for Observational Cosmology (CNOC) survey of selected rich clusters (Yee, Ellingson & Carlberg (1996), Carlberg et al. (1996)) allows such studies and comparisons over the approximate redshift range $0.2 \leq z \leq 0.6$.

The first cluster studied in detail using the CNOC database was Abell 2390 (Abraham et al. (1996), Yee et al. (1996)), at redshift 0.2279. In those papers, the cluster is seen to have well-defined and smooth radial gradients in galaxy color, morphology, and stellar population, showing that the cluster forms by galaxies continuously accreting from the

field. This accretion process appears to involve the cessation of star-formation, and passive evolution, creating a gradient in time since last star formation with clustocentric distance. The overall blue fraction of galaxies in the field around Abell 2390 is higher than in the zero redshift universe, both in the cluster and the nearby field, consistent with general aging of all galaxy populations.

One controversy in this area has been how severely galaxies are affected by accretion into a cluster: in particular, whether there is a population of merging or interacting infalling galaxies, whether infall disturbs the ISM enough to trigger a ‘starburst’² in an isolated galaxy, whether gas stripping may occur by the cluster IGM, and/or whether star-formation is halted on infall. We noted that we see little evidence of a population with excess star formation in Abell 2390, and advocated models of truncated star-formation to explain the observed radial gradients. Recently, it was pointed out to us that the issue of starbursting versus truncated star formation was carefully discussed in Newberry, Boroson & Kirshner (1990). Our conclusions here support and expand on their work, as well as complementing that in Abraham et al. (1996).

Clearly it is of interest to see whether the same can be said of other clusters, particularly those at even higher redshift, where the fraction of blue star forming galaxies is known to be higher (Butcher & Oemler (1984)). This paper provides a comparison with Abell 2390 by studying the rich cluster MS1621.5+2640 at $z=0.4274$. To allow easy comparison, we tabulate some of the parameters of these two clusters in Table 1. MS1621.5+2640 was chosen as the cluster in the CNOC database most likely to violate the passive truncated star formation model proposed for Abell 2390. We have data for a large number of members, and it was noted when the observations were being taken that line emission was common. As will be demonstrated, this impression was largely driven by the fact that most galaxies (field and cluster) at $z=0.42$ have higher star formation rates than those at $z=0.23$. We find that MS1621.5+2640 does not have an unusually large starforming population relative to the field.

A recent paper by Barger et al. (1996) studies the galaxy population distributions in various observational parameter spaces, for the inner regions of three $z=0.31$ clusters. They conclude that some 30% of the cluster galaxies have undergone a secondary burst of star formation in the previous 2 Gyr, and hence that infall causes a starburst. However, the difference between a galaxy with truncation following a period of rapid star formation, and

²One immediate cause for disagreement is in the definition of a ‘starburst’. Some authors seem to regard an Sc galaxy as a ‘starburst’. We will try to avoid some of this controversy by comparing our data with models with a simple star formation history which we will specify. This will allow others to decide whether any of the models are ‘starbursts’ or not for themselves.

one with simple truncation of star-formation is small in their key diagram ($H\delta$ versus color, as discussed in Abraham et al. (1996) and Newberry, Boroson & Kirshner (1990)), since the ‘active’ stage is very brief, and the ‘post-starburst’ stage (marked by strong $H\delta$ absorption) is longer lived and indistinguishable from the ‘post-truncation’ stage of a truncation model. In fact, they do not clearly test and evaluate the truncation model against a starburst model, and the number of active rapidly star forming galaxies is very small and may not be different from that of the field. Poggianti & Barbaro (1996) use the same data, but with independent models, coming to similar conclusions to Barger et al. (1996). We discuss this point in more detail in § 7.

In Balogh et al. (1997), we took a different approach to the above - looking at the [O II] $\lambda 3727$ Equivalent Width (EW) alone, but summing up all the CNOC cluster data. Again we found no evidence for a population with excess star formation relative to the field at the same redshift. Cluster members were shown to have a lower star formation rate than the field regardless of their color. The present detailed study of a single well sampled cluster is meant to complement that more broad-brush method.

Considerable interesting work on galaxy clusters at a range of redshifts around 0.5 (overlapping the redshift of MS1621.5+2640) has been published recently by the “MORPHS” collaboration (see Dressler et al. (1997) and references therein). They have used WFPC-2 data from HST to morphologically classify the objects in these clusters, and interpret these results as showing (amongst other results) that the formation of ellipticals in clusters predates the formation of the rich cluster, and also that S0 galaxies are generated in large numbers only after the cluster virialization. It will be exciting to join our results with those in the “MORPHS” papers, but we will not be doing so in this paper. It is difficult to determine which of our current sample of galaxies are morphologically S0, even using the concentration index discussed in § 2. The S0 class is a difficult one, involving objects with a wide range of bulge to disk ratio, and requires HST resolution to classify at these redshifts. We will be attempting to make this link using HST imaging of MS1621.5+2640 scheduled to occur over the second half of 1998.

The outline of this paper is as follows: We describe briefly the data and the line and morphology measurements in § 2, and go on to summarize the selection effects and biases in the data in § 3. Cluster membership criteria are explained in § 4. The changes in the various measured galaxy properties with location in the cluster are described in § 5, and ROSAT HRI X-ray observations are presented in § 6. Galaxy evolution models are described in § 7, and are used to interpret the observed gradients in galaxy properties. Finally, we present our conclusions in § 8.

2. Data and Measurements

The data in this paper were obtained as part of the CNOC project. The observational techniques and data reduction were the same as those for Abell 2390 described by Abraham et al. (1996). The reader is referred to that paper and also the CNOC data-reduction papers (Yee, Ellingson & Carlberg (1996), Yee et al. (1996)) for details of the experimental design. The data catalogue for this cluster is given in full in Ellingson et al. (1997).

The cluster MS1621.5+2640 was covered by central, northern and southern 9 arcmin by 7.9 arcmin fields, as it appears extended in the N-S direction, giving a total field of 9 arcmin by 23.3 arcmin. The central field was observed with 3 spectroscopic masks, the Southern with 2, and the Northern with 1. In all, 555 object spectra were obtained, covering the observed frame wavelengths 4650-6300Å (3260-4410Å in the cluster rest frame). From these, 277 reliable redshifts were determined, of which 112 galaxies were classified as cluster members. We discuss cluster membership in § 4 below.

The fields were imaged with Gunn g and Cousins R filters (with the latter calibrated in the Gunn r system), so that each galaxy has measures of position, Gunn r magnitude, Gunn g-r color, morphology, and several line indices from the spectra. Errors in the magnitudes and colors are discussed in Yee, Ellingson & Carlberg (1996) and Yee et al. (1996). The features measured, and used in this paper, are D4000 (the 4000Å break strength), and the equivalent widths of [O II] 3727Å, and Hδ. Indices and error estimates were calculated using the signal and noise vectors along with the bandpass definitions described in Abraham et al. (1996) and Balogh et al. (1997). In Figure 1, we show some example spectra with the locations of the index definitions plotted. These objects were chosen to illustrate some of the range of indices seen. In the top spectrum, there is a red galaxy with sizeable D4000, but also with possible weak [OII] in emission and Hδ in absorption. The middle spectrum shows how it is possible to obtain a negative Hδ index **without** actually having Hδ in emission. If the continuum shape is such that the continuum bands on either side of Hδ are low then the index will go negative. As will be explained later, the model spectra with which we will be comparing are measured in exactly the same way, so this unavoidable property of the index definitions should affect both data and models in the same way, making comparison fair. The bottom spectrum just shows a strongly star forming galaxy.

Updates to the measurement algorithm since the Abraham et al. (1996) paper include more robust error estimates, and also we have kept the two measures of the Hδ EW described in that paper separate, rather than combining them with a break at an EW of 2Å. We have only used the ‘wide’ (4082-4122Å) definition in this paper. This simplifies comparison with the models (see later), and does not seem to affect any of the conclusions. We have studied all of these line indices to investigate which are reliable measures and

good tracers of stellar population and age. As in Abraham et al. (1996), we have chosen to compare the H δ and D4000 measures with galaxy evolution models, and use the [O II] as a measure of current star-formation activity.

We have also performed morphology measurements on the images, as described in Abraham et al. (1994). In the original MOS images taken with the spectra, the image quality is poor in all regions except the center of the central field, so that reliable measures were possible only at small radii. This is due to a combination of poor seeing (>1 arcsecond) and also the poor off axis image quality of the MOS spectrograph. Additional higher resolution images were subsequently obtained with the SIS spectrograph and tip-tilt correction of the central field, and also used for morphology classification. D. Schade is making independent morphological measures (private communication), which will be used in a paper in preparation comparing with the line indices and color for the whole CNOC sample. HST imaging data for this cluster are scheduled to be taken, but are not yet available.

An archive of all the CNOC data, including the spectroscopic indices and the morphologies is being set up at the Canadian Astronomical Data Center.³

3. Completeness and Biases

The selection function for MS1621.5+2640 is plotted in Ellingson et al. (1997). This function covers all objects in the catalog - both field and cluster members. One of the strengths of the CNOC sample is that the field comparison sample can be drawn from objects observed in exactly the same way as the cluster sample. This greatly reduces any possible selection effects causing difference between the field and cluster sample. As will be described in the next section, we also restrict the redshift range of the field sample we use, in order to further reduce the possibility of any such selection biases.

There are a number of reasons why a galaxy of a given magnitude may or may not be in our spectroscopic sample. These are discussed in detail in Yee, Ellingson & Carlberg (1996), but to summarize the main points here, objects may be too faint for a successful redshift measurement (magnitude selection function), objects may be in a region that is too crowded for us to be able to put slits on all objects using only 2-3 masks (geometric selection), or objects may be lacking in strong features which are needed for redshift

³The CADC is part of the Dominion Astrophysical Observatory in Victoria, B.C., which is part of the Herzberg Institute of Astrophysics under the National Research Council of Canada.

measurement (color selection). In MS1621.5+2640, we were unable to allocate enough slits to cover all the galaxies above $r=22$, but have a high success rate for all such galaxies that we did allocate slits to (see figure 3 in Ellingson et al. (1997)). Thus although we are not complete, there should be no substantial biases in either the field or member samples above this magnitude. This claim is supported by the color selection functions shown in Ellingson et al. (1997) (figure 9). In figures 12-14 and figures 16-17, the small number of galaxies in the spectroscopic sample with magnitudes fainter than $r=22$ are plotted with different symbols to allow easy identification.

A second issue arises when we try to compare with the CNOC data on Abell 2390 at $z=0.2279$. Are we probing to about the same luminosity in the two clusters, and hence is it fair to make comparisons of the two samples without correction for this? The spectroscopic exposures for MS1621.5+2640 were roughly 3 hours in duration, while those for Abell 2390 were 1 hour long. Additional factors affecting the relative depth of the two samples are the CCD, grism and blocking filter efficiencies at the two different observed wavelengths. This leads to color selection effects in Abell 2390 starting to be significant at $r=21$ (Yee et al. (1996)), roughly a magnitude brighter than in MS1621.5+2640. Thanks to its lower redshift, it was easier to assign slits to a large fraction of the galaxies in Abell 2390, and so the spectroscopic sample is more complete, but comparing the points at which the magnitude selection functions for the two cluster drop by a factor 2 gives that the MS1621.5+2640 goes 1.3 magnitudes deeper in Gunn r than the Abell 2390 sample. The difference in distance modulus between the two clusters is 1.5 magnitudes, and so we feel it is not necessary to make any correction for this.

Finally there is the question of comparisons between MS1621.5+2640 and other clusters in the literature. The main comparison we will be performing is with the data of Couch & Sharples (1987), as analysed by Barger et al. (1996). Galaxies in their sample are drawn from a red ($R_F=20$) magnitude limited sample, which is close to the CNOC Gunn r . They do not publish details of their selection function, but given that their sample contains 112 galaxies from a projected radius from zero to 150 arcsec in three clusters at $z=0.31$, it is likely that they do not contain as many low luminosity galaxies as we do. This may be the cause of some of the differences between the conclusions in this paper and that of Barger et al. (1996) discussed later.

4. Cluster membership and field sample

Figure 2 shows the redshift space near the cluster in our data. Figure 3 shows that there is a well separated red sequence of cluster members. This red sequence can be defined

formally by sigma clipping of the cluster galaxy colors, which converges to a cut at around $g-r=1.2$ (see below). The distributions of red and blue galaxies on the sky are very different (see Figure 5), as in Abell 2390, with the red galaxies showing a clearly defined ‘cusp’ of virialized members. The blue galaxies are not found in the cluster center, and have a much less clear separation from the field at larger radii.

The curves plotted in Figure 2 represent 2.9 and 4.0 times the velocity dispersion of the cluster using the mass model of Carlberg, Yee & Ellingson (1997). The slightly odd value of 2.9σ was chosen to exclude the blue objects clumped near $z=0.435$ and projected radius of 600 arcsec. We take objects in the region between the 2.9 and 4 σ curves as our ‘near-field’ sample, and consider them separately in our analysis. These (presumably unvirialized) objects are bluer and have higher star formation rates than is typical even in the field. Galaxies outside of the 4 σ contour, but within the redshift range 0.37 to 0.50 are used as a field comparison sample. This is an arbitrary choice that gives roughly equal numbers of galaxies at redshifts on either side of the cluster, with a small enough redshift range to allow us to compare the important line features and make good color k-corrections. The results are not sensitive to the field redshift range used. We have a total of 112 cluster members with spectra, 47 galaxies lie in our field comparison sample, and 7 are near-field galaxies. As will be discussed later, for all the analyses involving spectral line indices, we further limit our sample using the error estimates of the line indices. This reduces the above numbers to 110 members, 45 field and 6 near field galaxies (see § 5.1 below).

Figure 3 shows the cluster members plotted on a color-magnitude diagram, and a color-radius diagram. The red sequence is fit by sigma clipping of the sample. The linear relations between color and magnitude or radius are shown and have slopes of 0.096/mag and $7.47 \times 10^{-4}/\text{arcsec}$ (or 0.125/log(arcsec)). Stanford, Eisenhardt & Dickinson (1998) demonstrate that the color-magnitude gradient is almost certainly caused by a correlation between galaxy mass and metallicity. Because of the small color change with magnitude (although somewhat larger than that found in Abell 2390, which was 0.024/mag), we make no color-magnitude correction in deriving the color-radius relation in Fig 3. As in Abell 2390, there is a significant color change with radius. For comparison, the slope in Abell 2390 is 0.079/log(arcsec). The same slope per kpc, scaled to $z=0.4274$, becomes 0.108/log(arcsec), consistent within the errors with that measured for MS1621.5+2640. Abraham et al. (1996) suggest that this color-radius relationship is due to an age-radius relationship, produced by the gradual accretion of field galaxies on to the cluster and their conversion into red, early type galaxies.

Figure 4 shows the colors of all galaxies as a function of redshift. To compare the field galaxies with the cluster members, we adopt a color k-correction given by $\Delta(g-r)=(g-$

$r+0.6)(z-0.4274)/(z+0.16)$, illustrated in the diagram with two arbitrary observed color cases. This family of straight lines is very close to the family of curves defined by different GISSEL models (Bruzual & Charlot (1993), and also § 7) in the redshift range covered by our field sample. As a check, we have verified that the correction produces no color-redshift slope to within the photometric errors in the data over the field sample range 0.37 to 0.50.

5. Galaxy population distribution

Figure 5 shows the distribution on the sky of galaxies of different types. Galaxies plotted as open symbols have higher spectroscopic errors, and are omitted from the plots based on those measures, as discussed in § 5.1.

In these plots we should note that the N-S distribution is uneven in part due to the fact that only one North field mask was used for spectra. This is obvious only in the field galaxy distribution: conversely, the higher concentration of member galaxies in the North may reflect a real asymmetry in the cluster population. The red galaxies, separated as discussed above, dominate the core region within 100 arcsec. The strong [O II] emitters may be somewhat less centrally concentrated than the strong H δ absorbers, consistent with star-formation truncation with infall.

The member galaxy distribution, particularly in the red, suggests that there may be a subgroup to the E of the core. We outline this group (A) in Figure 5, along with a box enclosing the cluster core (B). Group A in fact contains the formal ‘Brightest Cluster Galaxy’, although this galaxy is 3 arcmin from the cluster center defined by the X-ray centroid. The core group (B) coincides with the maximum in the X-ray flux contours (see § 6). We discuss the co-added spectra and group spectroscopic properties of the groups further in § 5.2.

5.1. Radial gradients

In all analyses involving spectroscopic line indices, we have selected the subset of the galaxies with H δ and [O II] errors less than 10.0Å. This just removes a few objects with extremely low S/N and leaves us with nearly the full sample. We use this subset for all the plots showing spectroscopic measures. The subset contains 110 of the 112 cluster members, 45 of the 47 in the full field sample, and 6 of the 7 near-field galaxies. As can be seen from the above numbers, this leaves our sample largely unchanged, and all the discussion of selection effects in Ellingson et al. (1997) and § 3 should still be appropriate. The resulting

mean error in the [O II] EW for cluster members is 2.0\AA , and the median error is 1.7\AA . The corresponding numbers for H δ are 1.3 and 1.1\AA . The D4000 errors are smaller proportional to the measurement (0.06 mean, 0.05 median), because this index involves averaging over many more pixels.

Figure 6 shows the radial gradients of these measures with error bars. We show the field galaxies distributed in redshift for clarity of comparison. This shows that there is a small foreground group or cluster near redshift 0.395.

These figures show trends that are very similar to those found for Abell 2390 by Abraham et al. (1996). The blue population grows with radius within the cluster. This gradient is also reflected in the distribution of the D4000 index. The [O II] line emission is seen only in the outer cluster (projected radius greater than 100 arcsec). For [O II] emission stronger than -15\AA , the cluster cannot be detected in redshift space. This is consistent with the idea of truncated star-formation in galaxies accreted from the field. If one excludes the ‘near-field’ objects (triangles), at no radius does the fraction of galaxies with strong [O II] exceed (or even match) that seen in the field. We also note here that an [O II] EW stronger than -15\AA is not unusual, even at zero redshift. This is demonstrated, for example, by Figure 11 in Kennicutt (1992). The majority of spirals of class Sc for instance have [O II] this strong or stronger. The H δ absorption also shows a decrease in the inner cluster, consistent with either pure truncation, or a period of rapid star formation followed by truncation, since the filling-in of Balmer absorption by emission during such a burst of star formation is very short in duration.

The near-field galaxies may be remarkable, although the small sample size makes any firm conclusions impossible. They appear to have extreme values of all four indices in Figure 6, even compared with the field. A similar result is obtained for the near-field galaxies in Abell 2390. This suggests that these galaxies, although supposedly not yet virialized in the cluster, may have been affected by the cluster in some way. It is perhaps appropriate at this point to mention that the projected radius alone of the near field objects put them at a distance of at least $2.3\text{ h}^{-1}\text{ Mpc}$ from the cluster core, more than twice the R_{200} ‘virialization’ radius (Carlberg et al. (1996)). Their velocity difference, if due to Hubble flow, would add another $20\text{ h}^{-1}\text{ Mpc}$ in quadrature to that distance. What we are calling ‘near field’ is probably a long way from the cluster core as measured in virial radii. A mechanism for increasing the star formation rate in galaxies at these radii is unclear, but the phenomenon is worth looking for in other clusters, to see if it can be established more definitely.

The strongest changes in the cluster population seen in Figure 6 occur at a radius of about 100 arcsec. Referring to Table 1, we can see this corresponds to about $350\text{ h}^{-1}\text{ kpc}$.

This is a larger physical radius than that found for such changes in Abell 2390 by about a factor 2. In Figure 7 we show the blue fraction of cluster members versus clustocentric radius. The blue fraction uses a cut $g-r=1.2$, and is defined for both cluster and field in the same way as the blue fraction shown for Abell 2390 in Abraham et al. (1996). We show the outer cluster values for Abell 2390 and Coma for comparison. The blue fraction in MS1621.5+2640 rises with radius and reaches the field value, whereas in Abell 2390 it does not. This difference could simply be due to the fact that the Abell 2390 data does not go out as far in units of R_{200} as the MS1621.5+2640 sample. We also show the higher value obtained when the near-field galaxies are included, for both MS1621.5+2640 and Abell 2390. The increase in blue fraction with redshift (Butcher & Oemler (1984)) is apparent, and has been described for the full CNOC cluster sample by Yee et al. (1995).

5.2. Group properties

Table 2 shows the mean properties of various subgroups. These quantities are derived from all the individual galaxies involved with no cutoff or weights imposed as a function of apparent magnitude apart from the one removing objects with errors in their line indices greater than 10\AA . These groups are also represented by co-added spectra, shown in Figure 8. The combined spectra are derived by adding the 10-15 brightest members of each group, to maximize the S/N. The mean indices for the objects summed to make the plot, and the groups as a whole, are not significantly different, so the spectral plots can be considered representative of the individual members of each group (although with much higher S/N). Note that the values listed in Table 2 do not, in general, have Gaussian-shaped distributions. There is no single number that measures their spread, or the significance of the differences. The main purpose of Table 2 is to allow typical values and trends to be seen at a glance.

Figure 8 shows that the oldest population groups (Groups A and B) in MS1621.5+2640 have spectra that differ from those in Abell 2390. The difference is most noticeable in the CN feature (rest wavelength 3875\AA , observed frame 5500\AA), and is an indication that the core Abell 2390 galaxies are older, as might be expected for a lower redshift cluster.

The central group B forms an arc of galaxies that may correspond to an X-ray feature (see § 6). These galaxies appear to be the oldest, but also have an unusually large velocity dispersion. The cluster is unusual in having the brightest member, cluster center, and gravitational arcs all in different locations. It is likely that the cluster is in a process of merging.

We also note that the group A galaxies have the properties and spectra of old populations: thus, they appear to be an evolved subgroup that is separate from the main cluster nucleus. They are not seen as a separate X-ray flux peak, so are not associated with any detectable hot gas of their own. The core subgroup, B, is slightly redder and more evolved (e.g. D4000). The mean redshift of the core group (B) matches that of the cluster members as a whole to better than 10 km/s. Group A has a mean redshift offset from the cluster mean by 270 km/s in the cluster rest frame. We suggest that these groups represent substructure, although we do not discuss the cluster dynamics in this paper.

Table 2 can also be used to determine whether there are systematic differences in say galaxy magnitudes between the member and field samples. Such differences could potentially invalidate the comparison of spectroscopic indices. As can be seen, there are no significant differences in mean luminosity between the blue member galaxies and blue field galaxies or the red member galaxies and red field galaxies.

5.3. Galaxy morphology

We have used the original MOS images for galaxy classification, as in Abell 2390. The image quality was not uniform across all fields, and, in practice, only the center field was useable for classification. We also have a higher resolution SIS image of the central 3 arcmin taken in better conditions, which was used for classification of the central cluster galaxies.

The concentration indices (Abraham et al. (1994)) are shown in Figure 9. The measures for the two different resolution images have different zero points as they are sampled differently and have different depths. We have renormalized the SIS image points to the MOS values based on two galaxies in common in the measures. There is an overall trend to less centrally concentrated galaxies (measured by C), with increasing radius, as seen in Abell 2390. There is a higher mean value (0.64) in the inner 100 arcsec, and a lower value (0.5) in the 100-300 arcsec radius range. The small numbers and uncertain offset between the two sets of measures make it difficult to draw more detailed conclusions, but the overall trend matches that seen in Abell 2390 in Abraham et al. (1996). The C values in Abell 2390 are higher and fall more slowly as a function of projected radius, but detailed comparison requires careful modeling of the effects of seeing and redshift on the C index, which we felt was not justified by the quality of the current imaging data for this cluster.

As mentioned in § 2, independent morphological measures are being made by D. Schade (private communication), and will be used in a paper in preparation comparing with the line indices and color for the whole CNOC sample. We are also obtaining HST images at

several radii for this cluster. Proper morphological statistics must await these data.

6. ROSAT HRI X-ray Emission

MS1621.5+2640 was observed with the ROSAT HRI July 28-30 1994 for a total of 44093 seconds. Figure 10 shows a grayscale representation of the HRI map with the locations of the galaxies with measured redshifts in the CNOC sample overlaid. Circles indicate cluster members, while plusses mark the positions of fore and background galaxies with redshifts. ‘Near-field’ galaxies are marked as crosses. The HRI data was smoothed with a gaussian of width $\sigma=8$ arcsec. Two very bright point sources are seen in the X-ray which are not associated with any cluster galaxy. They are almost certainly foreground stars or background AGN (both optical counterparts are unresolved on the digital sky survey). We note that the extended emission seen in this cluster in the EMSS catalog (Gioia et al. (1990)) could well be almost all due to the nearest of the unassociated point sources, given the comparatively poor spatial resolution of the Einstein IPC. There is however diffuse amorphous emission seen in the HRI image which is associated with the central group of galaxies in the cluster. The S/N is insufficient to say much more than that the emission is not strongly peaked on either the brightest galaxy of the central group, or the galaxy surrounded by a giant arc. This amorphous morphology contrasts strongly with the HRI data from A2390, presented by Pierre et al. (1996) which shows a much smoother profile. Other clusters with similar X-ray morphologies to MS1621.5+2640 have been described in the literature as examples of recent mergers (e.g. Ulmer & Cruddace (1982)). This evidence for lack of equilibrium in MS1621.5+2640 is supported by the following facts:

1. The brightest galaxy in the central regions is seen to have a luminous close companion in images taken with higher spatial resolution (unpublished CFHT data of S. Morris).
2. The bright arcs in this cluster are centered around the second brightest galaxy in the central group (Luppino & Gioia (1992), see also Gioia & Luppino (1994)).
3. The genuinely brightest galaxy in the cluster lies 3 arcmin to the east of the cluster center (in group A of Figure 5), and has no detectable X-ray emission associated with it.

A detailed analysis of the X-ray gas and mass profiles derived for most of the other CNOC clusters is given in Lewis et al. (1998). Unfortunately, the HRI data quality for MS1621.5+2640 was sufficiently poor, and also the evidence that the cluster X-ray gas was

not in hydrostatic equilibrium was so clear, that such analysis would not be appropriate for this cluster.

7. Application of spectrum models

As in Abraham et al. (1996), we have generated GISSEL models (Bruzual & Charlot (1993)) for the redshift of the cluster (0.4274) and measured the same spectral line and feature measurements as was obtained for the observed spectra. Specific upgrades and changes since that paper include:

1. We are now using the Bruzual and Charlot 1996 models (GISSEL96)⁴, copied from `gemini.tuc.noao.edu`. These allow a range of metallicities to be included.
2. These models are then shifted to the appropriate redshift and converted into IRAF format files, which are measured with exactly the same code as was used for the real data.
3. A correction has been computed for the fact that the new GISSEL96 models have lower spectral resolution than the observed data. Real CNOC spectra were blurred out to match the model resolutions, and the resulting changes in the indices measured. Details on this will be given in a paper in preparation by Balogh et al., but roughly, this amounts to adding 1.7Å to the GISSEL model H δ values measured by the code.
4. Colors were measured using the IRAF ‘sbands’ task. Magnitude zero points were computed (also using this task but on appropriate A and G type stars) to calibrate g-r.
5. A Salpeter IMF slope was used throughout. There are claims in the literature that this IMF may in fact be universal (Wyse (1997)). We will show one model where we imposed a ‘high’ low mass cutoff at 2.5 solar masses, but otherwise all models include stars from 0.1 to 125 solar masses.
6. For Abell 2390, the models were reddened by E(B-V) of 0.075 (E(g-r) of 0.084) using the Burstein & Heiles (1982) dust maps. Higher resolution maps are now available from Schlegel, Finkbeiner & Davis (1998), which give an E(B-V) of 0.11074 for

⁴For experts, the majority of the models run used the spectral energy distribution files of the form `bc96_0pxxxx_sp_ssp_kl96.ised`, where `xxxx` is a number between 0004 and 1000 related to the metallicity (0200 being solar).

Abell 2390 and $E(B-V)$ of 0.03143 for MS1621.5+2640. This latter value was small enough that we have made no correction to these models for galactic reddening.

Two simple star formation histories were considered:

- A 1 Gyr period of constant star formation starting at time 0, followed by complete cessation of star formation.
- An exponentially decaying star formation rate starting at time 0, with a time constant of 4 Gyr (chosen to be significantly different from the previous model).

These are meant to roughly represent elliptical and late-type spiral galaxies, respectively. The choices are arbitrary, but do produce spectra that roughly match present day spirals and ellipticals at late times. Obviously many far more complex star formation histories are possible, and indeed may be more realistic, but it is intended that these two simple cases will help illustrate the trends in the data. Figure 11 shows how the two models evolve in the color- $H\delta$ and color-D4000 planes for solar metallicity. Dots are marked at 1,2,3...20 Gyrs. It can be seen that the two tracks combine at early and late times (although note that the spiral model does not reach the elliptical one until after 20 Gyrs for this model, which is considerably longer than the age of the universe at a redshift of 0.4274). Between these two asymptotes, the spiral model spends a long time with fairly blue colors, very slowly evolving towards the red. The elliptical model spends a Gyr or so with elevated $H\delta$ absorption, but rapidly evolves to red colors and low $H\delta$ (high D4000).

It should be noted that both of these models involve periods of time when most people would describe them as ‘starbursts’. The elliptical model in particular forms all its stars rapidly, and then spends a period of 1-2 Gyrs looking like things generally called ‘poststarburst’ galaxies in the literature. Similarly, the spiral model in its first few Gyrs spends time looking like a ‘starburst’ or ‘poststarburst’ galaxy according to many definitions. As explained in a footnote earlier, we would like to minimize the use of these terms, and leave the reader to map from our model curves to their own terminology.

Models involving truncation of star formation in a spiral model basically just jump across at constant $H\delta$ from the spiral track to the elliptical track. Models including a burst of star formation added on to a spiral model spend a very short time looping around to very blue colors and low $H\delta$ (Barger et al. (1996), Poggianti & Barbaro (1996)), but then move rapidly to parallel the elliptical track closely. Without adding in a modified IMF, there are no models that fill in the region of red colors and high $H\delta$. (We will discuss this further in the next section).

We have also explored using the entire spectral model in comparison with the observations, rather than measurements of only a few strong individual features. This is most simply done by cross-correlation. The peak height and width is a measure of the match: in practice the lower spectral resolution of the models makes this approach less sensitive than it might be, and we do not achieve any greater sensitivity with this approach compared using the most reliable individual features as we have done.

7.1. Modeling of the Observed Galaxy Population Gradients

In Figure 12 we show the changes in the color- $H\delta$ plane as a function of radial distance in the cluster. Moving from optimistic to pessimistic, we note first that the GISSEL96 models with a simple star formation history are a good match to the cluster data at radii of >300 arcsec. However, at smaller radii, the red galaxies all seem to have $H\delta$ index too high for their color. Below we will explore some possible ways to explain these objects, but will basically rule out all the simple explanations that occur to us. This is not simply a case of a few extreme galaxies, but seems to apply to **all** the galaxies in this color range. The radial trends mentioned earlier can also be seen in these plots, with the ‘spiral’ population rapidly disappearing as one moves inwards in projected radius.

Figure 13 shows what seems to us to be astonishingly good agreement between these simple models and the data for the color-D4000 plane. In particular, there is no evidence for large amounts of reddening (which would be seen as a shift away from the model line towards larger g-r), and there is a clear separation in the data between objects matching the models with ongoing star formation, and models where the star formation was truncated at some earlier time at $g-r \sim 1.2$. Figure 14 shows that the excess of ‘ $H\delta$ strong’ objects can be seen (especially in the 100 to 300 arcsec radial bin) even when D4000 is used rather than g-r color. This seems to further exclude dust as a reasonable explanation, and also eliminated problems in our magnitude calibration (either of the data or the models) as the source of the mismatch. The data looks more scattered in this plot, as the D4000 index has larger error bars than the g-r color, and also the D4000 index is susceptible to systematic problems in the spectroscopy not included in the formal random error bars, such as occasional zero order or cosmic ray contamination, misplaced slits, inaccurate extraction from the 2D spectral frames, etc.

An additional interesting fact about the red galaxies with significant $H\delta$ absorption, is that they tend to be the lower luminosity ones. This is illustrated in Figure 15. It is particularly clear in the inner 100 arcsec panel, but in general the red galaxies with $H\delta$ greater than 5\AA are all fainter than 20 in r. It should also be noted though that our

spectroscopic sample begins to be biased in favour of strong line emitting galaxies at around Gunn $r=22$ (see § 3), as it is easier to derive redshifts for these objects. Conversely, this will tend to remove objects from our sample with red colors and weak absorption features fainter than $r=22$.

Although the GISSEL96 models do not include line emission, we also show the color-[O II] plane in Figure 16 for completeness. It can be seen that the red objects with excess $H\delta$ index over that in the models basically show no [O II] line emission at all. [O II] is seen exclusively in objects bluer than $g-r=1.2$. Comparison of the field sample with the outer cluster region also re-emphasizes our earlier point that at no radius is an excess of [O II] emitters seen in the cluster compared with the field, unless the near field objects are included as members.

Finally in Figure 17 we show all the cluster members plotted over the two simple models. This emphasizes the dramatic break between objects with ongoing versus truncated star formation at $g-r=1.2$, and also shows the general excess in the $H\delta$ index of all the red galaxies relative to the models. The eye suggests that there may be two populations of red galaxies - one with $H\delta$ less than 4\AA , and a smaller, more extreme, group with $H\delta$ greater than 4\AA . The star-forming and non-star-forming populations can be roughly divided at a $g-r=1.2$ color, and so their spatial distributions can be read off from Figure 5. The blue galaxies are uniformly spread in projected radius, and are not clumped towards the center, suggesting they are not yet virialized. However, the RMS velocity of the blue galaxies from Table 2 is not significantly different from that of the red galaxies. There is some evidence for reddening of the red galaxies from the D4000 versus $g-r$ plot by about 0.1-0.2 in $g-r$, but this is not enough to explain the discrepancy in the top plot.

We will now consider a few more extreme models to see if we can explain the above mismatch. We show some of these in Figure 18. First, in the top left panel we test the effects of spectral resolution on our measurements. For the comparison model, the 3520-7400 \AA region uses GISSEL models based on the spectra from stars in the Jacoby, Hunter & Christian (1984) atlas. Apart from some significant differences for blue objects with high $H\delta$ index, the higher spectral resolution models match our corrected low resolution ones. Resolution effects certainly do not move the models over into the region of red colors and high $H\delta$ index. In the top right panel we show the effects of reddening. Reddening of $A_V=1$ would certainly allow the simple models to explain the observations, but such massive amounts of reddening, for a large fraction of the early-type population in the cluster, is unreasonable, especially given the D4000 versus $g-r$ plots in Figure 13. In the lower left panel we show the two most extreme metallicity models in the GISSEL96 suite. Even 5 times solar metallicity (a model which Bruzual and Charlot suggest should be treated with

caution in their documentation accompanying the GISSEL96 models) the g-r color does not move far enough to the red to match the data.

Finally, prompted in part by Charlot et al. (1993), we show in the lower right panel a model with the IMF truncated below 2.5 solar masses. This is rather extreme truncation, but should illustrate the possibilities. There have been suggestions in the literature for some time that the IMF in ‘starburst’ galaxies may be anomalous (see references in Charlot et al. (1993)), with diminished or no low mass stars. Charlot et al. (1993) show that in such cases, if the period of rapid star formation involves a significant fraction of the galaxy’s stars, then a galaxy can spend up to a Gyr with unusually red colors and large D4000. As can be seen in Figure 18, the time spent with very red g-r colors is very short for this particular model, and the time with simultaneously large H δ index is even shorter. In this (again possibly extreme) example, the model in fact spends a long time with unusually high H δ and colors blueward of g-r=1 - a region unpopulated by galaxies in our data. In summary, we do not feel that varying GISSEL96 model resolution, reddening, high metallicity, or bursts with unusual IMFs will produce a good match to our observed red galaxy distribution in H δ index versus g-r.

One caveat that should certainly be repeated here is that the H δ index we measure is just that - an index. As can be seen, it is predicted to go negative at late ages, and indeed several red galaxies do have such negative indices. This does not mean that they have H δ in emission, but just that the continuum bands on either side of the line are more depressed than the central band (see Figure 1). We have not yet investigated the details of what molecules and ions dominate the absorption in this complex region, but clearly this deserves further study.

7.2. Comparison with Barger et al.

As described earlier, Barger et al. (1996) present similar measurements for a sample of 3 clusters at z=0.31. By combining the data from these clusters, they end up with a sample of about the same size as ours (112 members total, compared to our 110 for MS1621.5+2640). The cluster members for their sample range in projected radius from zero to 150 arcsec at z=0.31, and so generally correspond to our inner region in Figures 12-16. The error bars plotted for H δ in Couch & Sharples (1987) are in general considerably larger than ours - typically 2-4Å, although Barger et al. (1996) claim the 1 σ errors are in fact typically 1Å. Barger et al. (1996) go on to model galaxy evolution using an earlier version of the GISSEL models and also add in the effects of line emission. They then quantitatively compare the numbers of objects in specific regions of their diagrams (e.g. their Figure 5)

with the expected numbers from the models, given the time spent in each location. From this they conclude that around 30% of the cluster members had a secondary burst of star formation. We show their dividing lines in Figure 19, along with the numbers of galaxies in each region in our data and in the Barger et al. (1996) data. There are a number of comments we would like to make about this comparison:

- We see considerably fewer ‘SB’ (‘starburst’) class objects in our cluster.
- We also see somewhat fewer ‘HDS’ ($H\delta$ strong) objects. In general, none of our current (simple) GISSEL96 models can match these, either as objects with recently truncated star formation, or with an additional burst of star formation. Although they do not explicitly plot the models and the data together, we note that the GISSEL models shown in Barger et al. (1996), in our opinion, also have trouble reproducing the objects with red (B-V) colors and high $H\delta$. The problem was also reported by Poggianti & Barbaro (1996).
- We do see a comparable number of objects in the ‘PSG’ (‘Post-starburst’ galaxy) region, but note that, given our error bars, these points are all consistent with our two simple models that are intended to match ‘normal’ elliptical and spiral galaxies. At some level this is semantics, in that our elliptical model does indeed involve a ‘burst’ of star formation, making up the whole galaxy. However, the ‘PSG’ points in our data set do not lie far (in terms of the errors) from the ‘spiral’ track with its smooth decay in star formation. Objects in this region certainly are showing signs of recent star formation - indicating a younger age, later formation time than the majority of the cluster members.
- Possibly due to our smaller error bars, it is easier to (subjectively) identify populations of points that seem to go together. If we modify the Barger et al. (1996) dividing lines, to use those shown in Figure 19 as dotted lines, we then remove objects matching our simple early-type galaxy model from the HDS category, and also remove some objects consistent with our simple late-type galaxy model from the SB and PSG category. Doing this generates the numbers in brackets in the plots, and leaves rather few objects in our redefined ‘PSG’ and ‘HDS’ categories.
- For comparison, we also plot the distribution and numbers of galaxies in our field sample. Given the uncertainties from the small sample size, the main differences are (a) a larger early-type fraction in the cluster (no surprise at all), and (b) possibly an excess of ‘HDS’ galaxies in the cluster, although whether this ratio should be taken relative to the whole sample, or alternatively just the other red galaxies seem debatable to us.

Poggianti & Barbaro (1996) perform an identical analysis to Barger et al. (1996), using the same data, but an independent galaxy modeling code. They reach similar conclusions to Barger et al. (1996), but also explicitly state that none of their models (including a variety of bursts) can explain the objects with $B-R > 2.3$ and strong $H\delta$. Plotting their models over the Barger et al. (1996) data confirms this. They also claim that their models can not reproduce the large $H\delta$ values seen with simple truncation of star formation and no burst. Obviously, we do not agree with this conclusion. One possible reason for the disagreement might be that our approach of using identical code on both the data and the models (with a correction derived for the differing spectral resolution) is more robust. However, it must also be admitted that we do not include the effects of $H\delta$ infill by gaseous emission in our model plots, which Poggianti & Barbaro (1996) do.

Bringing in some IR data, Barger et al. (1996) and Barger et al. (1998) both look at the evolution of the K-band luminosity function of the early-type galaxies with redshift, and find no significant changes beyond passive evolution between $z=0$ and 0.56. This seems to support a model in which there is no significant additional star formation in this population.

7.3. Galaxy ages and metallicities

In principle, comparison of the observed galaxy distributions with the GISSEL96 models should allow rough determination of the galaxy ages. In practice, as is well known, age and metallicity are inextricably intertwined in most such comparisons. To illustrate this problem, we show in Figure 20 the GISSEL96 D4000 and $H\delta$ indices plotted against time. Overlaid on the model curves are the observed distributions of the cluster members. For D4000, the well defined edge around a value of 2.3 in turn leads to a fairly well defined age, if the metallicity is known, or alternatively a well-defined metallicity if the age is known. For solar metallicity, this value of D4000 corresponds to an age of 7.5 Gyr. For 2.5 times solar, the corresponding age is 3 Gyr. Depending on one's preferred cosmology, one might wish to invert this problem, and assume an age to derive typical metallicities for the red galaxies⁵.

⁵After this paper was submitted a preprint from van Dokkum et al. (1998) came out that uses the width of the elliptical and S0 sequences in a color magnitude diagram of the cluster MS1358.4+6245 ($z=0.328$, also in the CNOC sample) to set limits on the star formation histories of these two populations. They use analytical models for the evolution in color as a function of time, and derive that star formation in the ellipticals ceased at $z \geq 0.6$, while the S0 population in the outer parts of the cluster experienced star formation up to the epoch of observation.

One way to try to break this degeneracy would be by using some of the other line indices (Worthey (1994)), but our other well studied index ($H\delta$) has the problem that the entire red population seems to have high $H\delta$ index relative to the models, making using the low edge of the distribution (near -2 \AA) very questionable. We have not looked in any detail at using other line indices from our spectra, or alternatively folding in the g-r colors. This latter would obviously also require estimation of the reddening in each galaxy.

8. Conclusion

We list below the main conclusions from the paper.

1. The blue population and general change in cluster membership begins at a radius of 100 arcsec (or approximately $350 h^{-1} \text{ kpc}$). This is a larger linear radius than in Abell 2390 (approximately $150 h^{-1} \text{ kpc}$). Thus, the cluster core is considerably less compact in MS1621.5+2640.
2. There is an evolved subgroup some 3 arcmin to the E containing the true ‘BCG’.
3. The near-field galaxies may have enhanced star-formation. These are at very large radii (greater than $2 h^{-1} \text{ Mpc}$), and the mechanism for this enhancement remains unclear.
4. A gradient is seen in the g-r colors of the red galaxies with projected radius, which we interpret as a gradient in the time since last star formation. This in turn fits well with models where the cluster formed by gradual accretion of field objects, which in turn then evolve (spectroscopically) into early-type galaxies.
5. The overall blue fraction is higher than at lower redshift, both in the field and the cluster. The outer cluster blue fraction matches that of the field, with the exception of the near-field (blue) galaxies.
6. We find no signs of extensive star-formation in the cluster compared with the field. Compared with the field, the average $[\text{O II}]$ is weaker in the cluster, as is $H\delta$, and the galaxies are redder. This is consistent with simple truncation of star-formation as galaxies are accreted.
7. Detailed comparisons with GISSEL96 models show a good match in general except for an odd excess in $H\delta$ index for all galaxies redder than $g-r=1.2$. Various attempts to explain this excess (resolutions differences, reddening, metallicity, truncated IMFs) were not successful, but certainly deserve further study.

8. At this redshift, the models allow us to distinguish two galaxy populations in the cluster: one best modeled with steadily decreasing star-formation, similar to that seen in spirals in the field, and another in which star-formation has terminated.

To summarize further, and also indulge in some speculation, the above data, combined with that on Abell 2390, seems to be consistent with a fairly passive process of cluster formation. Galaxies are gradually accreted from the field, with no good evidence for a large burst of star formation as they are virialized into the cluster. The star formation in the galaxies begins shutting down at very large radii (well outside the virial radius), for reasons that remain unclear. However, there is evidence for recent (within the last 1-2 Gyr) star formation even in the inner 100 arcsec of the cluster. This star formation is mostly seen in the lower-luminosity early-type galaxies in the cluster core. This suggests to us that the shut down process for star formation could well be some combination of stripping of gas from the outer parts of the galaxies as they fall in, followed by gradual exhaustion of the gas in the inner parts. This would allow the remnants of star formation to be still visible in galaxies seen in the core. One hundred arcsec at this redshifts is $350 h^{-1}$ kpc, which would take 0.4 Gyr to cross, going at the cluster velocity dispersion speed of 850 km/s. The fact that the inner galaxies with stronger H δ have lower luminosities could either imply that they have had different dynamical histories (i.e. the more luminous galaxies either formed there or fell in earlier), or that the lower luminosity galaxies were more gas rich, and hence more able to hang on to their star formation in the presence of stripping. One should also remember the general trend that more luminous galaxies even in the field tend to have formed their stars earlier than the lower luminosity ones.

We would like to thank Amy Barger for helpful comments on an earlier draft of this paper. The data used in this paper form part of the CNOC study of intermediate-redshift clusters. We are grateful to all the consortium members, and to the CFHT staff (particularly the Observing Assistants Ken Barton, John Hamilton and Norman Purves) for their contributions to this project.

REFERENCES

- Abraham, R. G., Valdes, F., Yee, H. K. C., & van den Bergh, S. 1994, *ApJ*, 432, 75
- Abraham, R.G., Smecker-Hane, T. A., Hutchings, J. B., Carlberg, R. G., Yee, H. K. C., Ellingson, A., Morris, S. L., Oke, J. B. & Rigler, M. 1996, *ApJ*, 471, 694
- Balogh, M. L., Morris, S. L., Yee, H. K. C., Carlberg, R. G. & Ellingson, E. 1997, *ApJ*, 488, L75
- Barger, A. J., Aragon-Salamanca, A., Ellis, R. S., Couch, W. J., Smail, I. & Sharples, R. M. 1996, *MNRAS*, 279, 1
- Barger, A. J., Aragon-Salamanca, A., Smail, I., Ellis, R. S., Couch, W. J., Dressler, A., Oemler, A., Poggianti, B. M. & Sharples, R. M. 1998, *ApJ*, in Press, astro-ph/9801112
- Bruzual, G. & Charlot, S. 1993, *ApJ*, 405, 538
- Burstein, D. & Heiles, C., 1982 *AJ*, 87, 1165
- Butcher, H. & Oemler, A. Jr. 1984, *ApJ*, 285, 426
- Carlberg, R. G., Yee, H. K. C., Ellingson, E., Abraham, R., Gravel, P., Morris, S. L. & Pritchett, C. J. 1996, *ApJ*, 462, 32
- Carlberg, R. G., Yee, H. K. C. & Ellingson, E. 1997, *ApJ*, 478, 462
- Charlot, S., Ferrari, F., Mathews, G. J. & Silk, J. 1993, *ApJ*, 419, L57
- Couch, W. J. & Sharples, R. M. 1987, *MNRAS*, 229, 423
- Dressler, A., Oemler, A. Jr., Couch, W. J., Smail, I., Ellis, R. S., Barger, A., Butcher, H., Poggianti, B. M. & Sharples, R. M. 1997, *ApJ*, 490, 577
- van Dokkum, P. G., Franx, M., Kelson, D. D., Illingworth, G. D., Fisher, D. & Fabricant, D. 1988, *ApJ*, In Press, astro-ph/9801190
- Ellingson, E., Yee, H. K. C., Abraham, R. G., Morris, S. L., Carlberg, R. G., Smecker-Hane, T. A. 1997, *ApJS*, 113, 1
- Gioia, I. M., Maccararo, T., Schild, R. E., Wolter, A., Stocke, J. T., Morris, S. L. & Henry, J. P. 1990, *ApJS*, 72, 567
- Gioia, I. M. & Luppino, G. A. 1994, *ApJS*, 94, 583

- Jacoby, G. H., Hunter, D. A. & Christian, C. A. 1984, *ApJS*, 56, 278
- Kennicutt, R. C. 1992, *ApJ*, 388, 310
- Lewis, A. D., Ellingson, E., Morris, S. L. & Carlberg, R. G. 1998, *ApJ*, Submitted.
- Luppino, G. A. & Gioia, I. M. 1992, *A&A*, 265, 9L
- Newberry, M. V, Boroson, T. A. & Kirshner, R. P. 1990, *ApJ*, 350, 585
- Pierre, M., Le Borgne, J. F., Soucail, G. & Kneib, J. P. 1996, *A&A*, 311, 413
- Poggianti, B. M. & Barbaro, G. 1996, *A&A*, 317, 379
- Schlegel, D., Finkbeiner, D. & Davis, M. 1998, *ApJ*, In Press. See <http://astro.berkeley.edu/davis/dust/index.html>
- Stanford, S. A., Eisenhardt, P. R. & Dickinson, M. 1998, *ApJ*, 492, 461
- Ulmer, M. P. & Cruddace, R. G. 1982, *ApJ*, 258, 434
- Worthey, G. 1994, *ApJS*, 95, 107
- Wyse, R. F. G., 1997 *ApJ*, 490, L69
- Yee, H. K. C., Sawicki, M., Ellingson E., & Carlberg R. G. 1995, in *ASP Conf. Ser. Vol. 86*, “Fresh View of Elliptical Galaxies”, ed. A. Buzzoni, A. Renzini & A. Serrano
- Yee, H. K. C., Ellingson E., Carlberg R. G. 1996, *ApJS*, 102, 269
- Yee, H. K. C., Ellingson E., Abraham, R. G., Gravel, P., Carlberg R. G., Smecker-Hane, T. A., Schade, D. & Rigler, M. 1996, *ApJS*, 102, 289

Table 1. Cluster Comparison of A2390 and MS1621.5+2640

Property	A2390	MS1621.5+2640
Redshift	0.2279	0.4274
Scale ^a (arcmin/h ⁻¹ Mpc)	6.897	4.615
Area Surveyed (arcmin)	46 × 7 (E-W)	9 × 23 (N-S)
Area Surveyed (h ⁻¹ Mpc)	6.7 × 1.0	2.0 × 5.0
L _X (h ⁻² ergs/s, 0.3-3.5 KeV)	4 × 10 ⁴⁴	5 × 10 ⁴⁴
Velocity Dispersion (km/s)	1095	841
R ₂₀₀ ^b (h ⁻¹ Mpc)	1.51	0.98
M _v ^b (h ⁻¹ M _⊙)	2.6 × 10 ¹⁵	0.98 × 10 ¹⁵

^aq₀=0.1

^bsee Carlberg et al. (1996)

Table 2. 1621+246 mean group properties

Group	#	g-r	D4000	H δ (\AA)	[O II] (\AA)	R ^a ($''$)	Δz	m_R
Blue (g-r<1.2)	38	0.82	1.54	5.1	-15	320	0.0038	21.3
Red (g-r>1.2)	72	1.55	2.09	1.2	1	210	0.0041	20.8
HDS (H δ >5)	25	0.99	1.64	6.9	-13	319	0.0041	21.4
[O II] ([O II]<-15)	15	0.69	1.40	6.2	-30	330	0.0043	21.8
Group A	10	1.47	2.00	1.1	0	215	0.0034	20.8
Group B	12	1.64	2.19	0.7	0	31	0.0069	20.7
Radius<100''	19	1.66	2.22	1.3	1	48	0.0059	20.8
Radius<100'' g-r<1.2	0	—	—	—	—	—	—	—
Radius 100''-300''	59	1.28	1.87	2.4	-4	208	0.0037	20.9
Radius 100''-300'' g-r<1.2	20	0.81	1.53	4.5	-16	202	0.0042	21.1
Radius>300''	32	1.12	1.75	3.7	-7	439	0.0029	21.3
Radius>300'' g-r<1.2	18	0.83	1.54	5.8	-13	451	0.0034	21.5
Near field	6	0.49	1.25	7.3	-34	636	0.0076	21.6
Field	45	1.06	1.62	4.0	-18	(436)	—	21.1
Field g-r<1.2	27	0.80	1.42	5.1	-28	(470)	—	21.4
Field g-r>1.2	18	1.43	2.01	2.3	-3	(384)	—	20.7

^aProjected distance in arcsec from cluster center

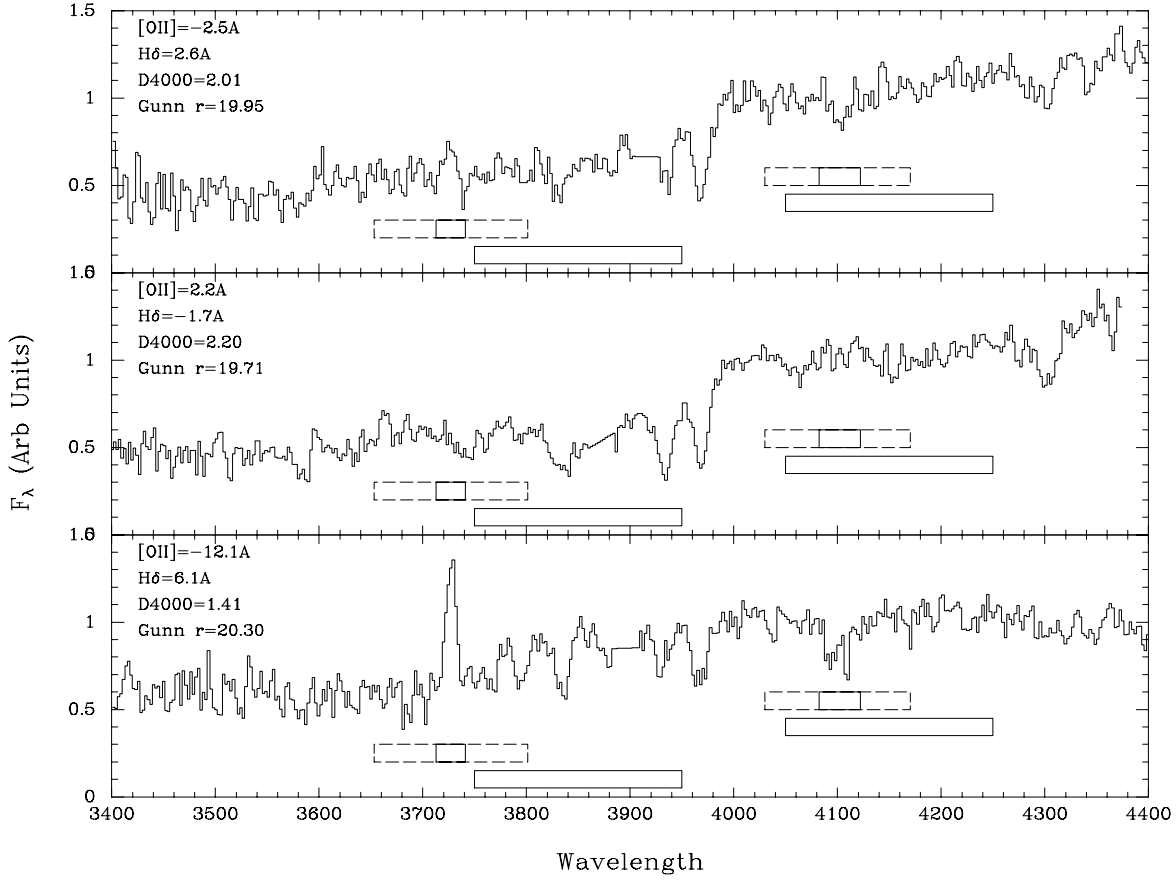


Fig. 1.— Examples of line index definitions. The solid box centered at 3727Å is for $[OII]$, the dashed boxes on either side show its continuum regions. The solid box centered at 4101Å is for $H\delta$, with similar continuum bands. The $D4000$ index is defined as the ratio of the fluxes in the two larger solid boxes centered around 3850Å and 4150Å . The three objects plotted (rest frame wavelengths), from top to bottom are: (a) a red galaxy showing faint signs of star formation including possible $[OII]$ emission, and weak $H\delta$ absorption. (b) a ‘normal’ red galaxy. (c) A strongly star forming galaxy. The line index values for each galaxy are shown in the top left corners. The straight line segment just blue of the $CaII$ absorption is a residual from correction of the strong night sky line at 5577Å in the observed frame.

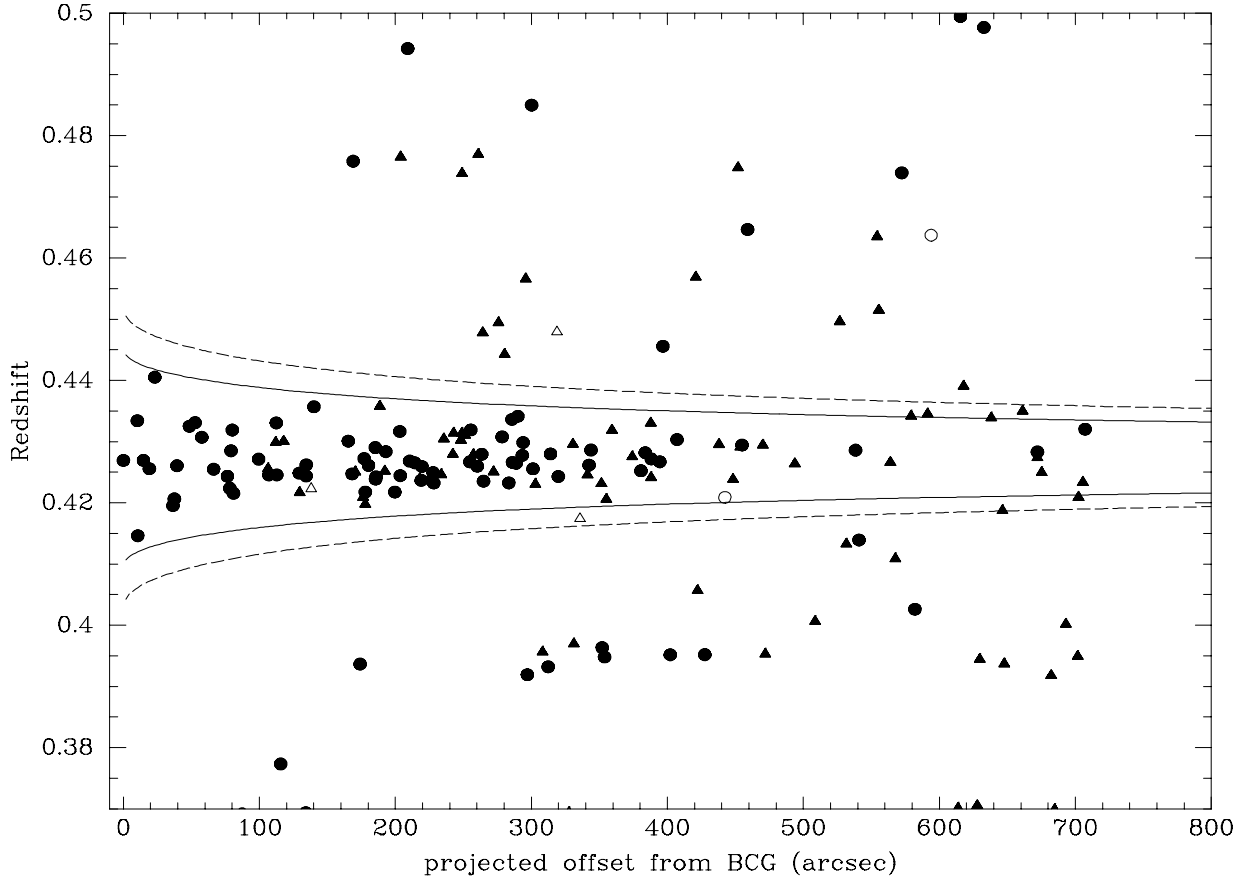


Fig. 2.— Galaxy redshifts versus projected distance from cluster center, separated into red (circles $g-r > 1.2$) and blue (triangles, $g-r < 1.2$). The curves are 2.9 and 4σ lines which we adopt to define membership, as discussed in the text. Open symbols are galaxies with poor S/N which are not used for the plots involving spectroscopic measurements.

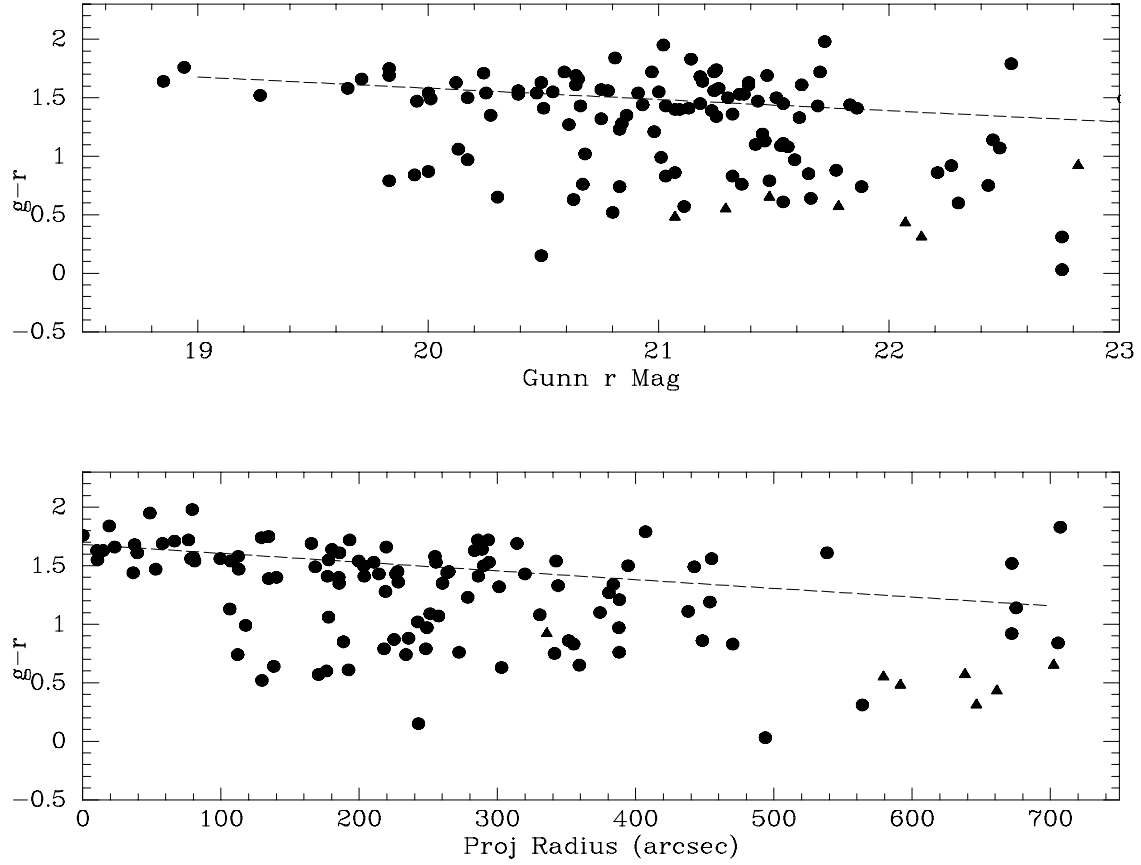


Fig. 3.— Variation of cluster galaxy color with magnitude and clustocentric projected distance. The lines are linear fits to them with sigma-clipping to isolate the red population. The triangles are the near-field galaxies. See § 3 for a discussion of the unbiased magnitude range.

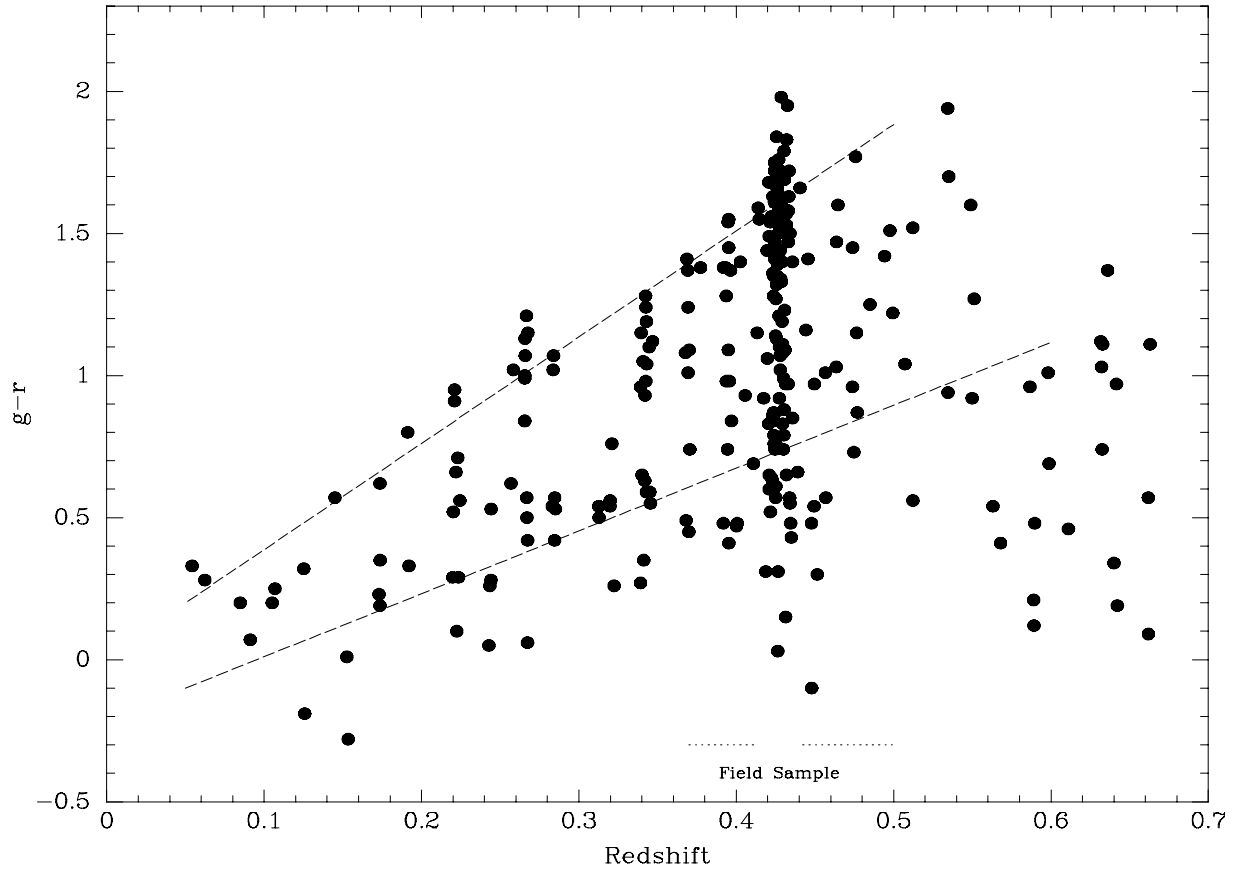


Fig. 4.— Colors of all galaxies as a function of redshift. The cluster and its red population stand out clearly. Other structure can be seen at lower redshifts. The redshift range used for the field galaxy sample is indicated. The lines illustrate the color correction made to the field galaxies for comparison with the cluster galaxies.

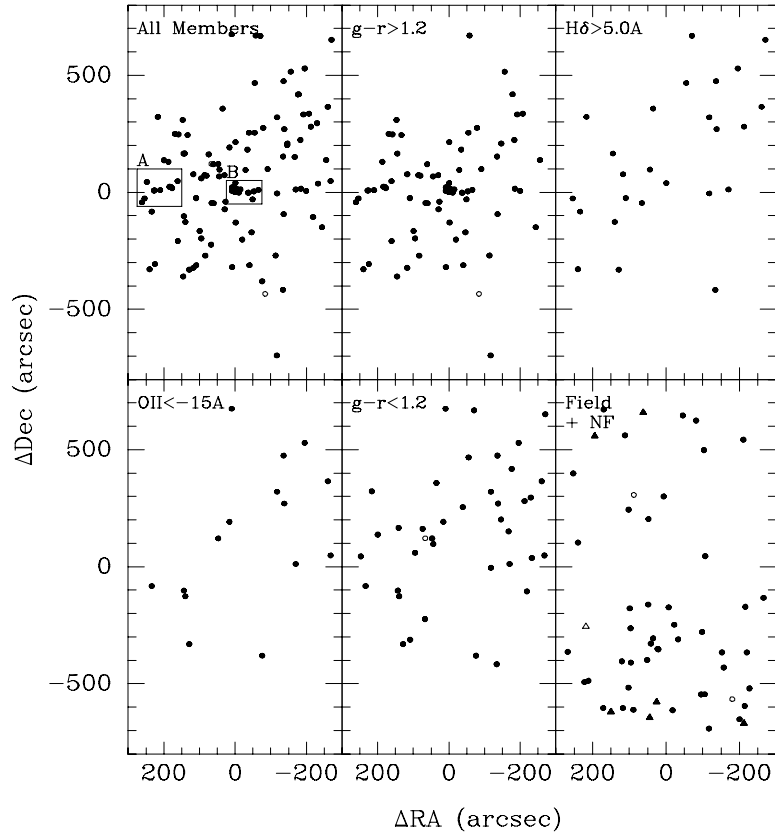


Fig. 5.— Distribution of subsets of cluster galaxies and the field sample. The two subgroups discussed are outlined. Open symbols are galaxies with poor S/N which are not used for the plots involving spectroscopic measurements. Near field galaxies are plotted as triangles.

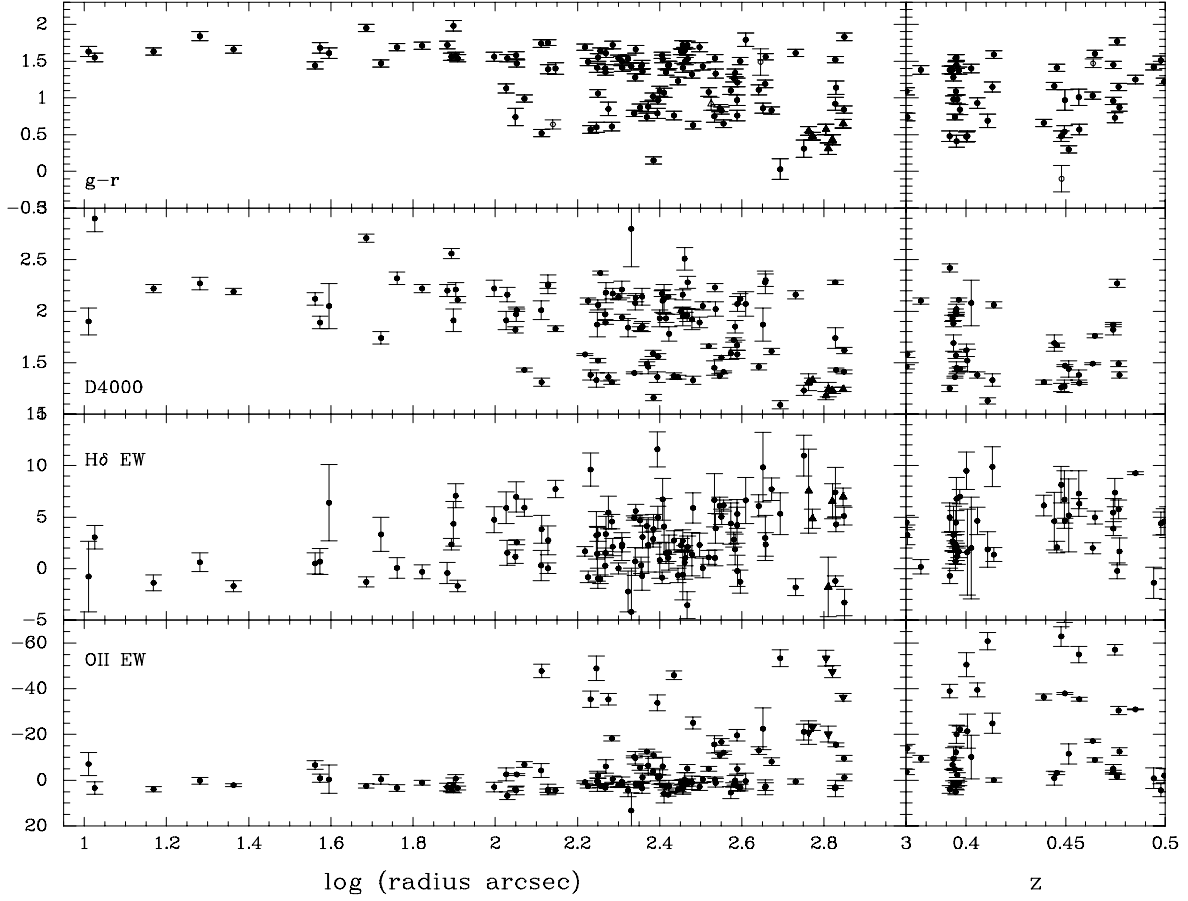


Fig. 6.— Distribution of color and spectroscopic properties with clustocentric projected distance. Triangles are the near-field galaxies. The field samples are plotted against redshift for comparison. For the top plot, this includes the full sample, the lower three plots only show the subset with high quality spectroscopic indices. Objects with large errors in line index are marked at open symbols in the top panel.

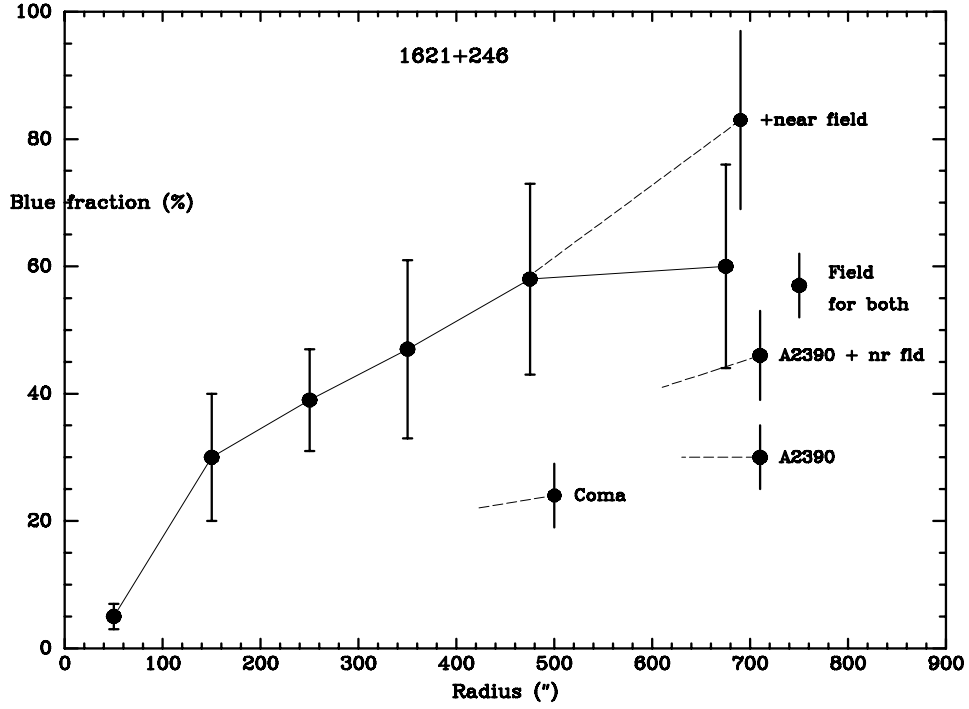


Fig. 7.— Blue fraction as defined by the σ -clipped red population (see Figure 3) as a function of projected radius. The field value, and the value including the near-field galaxies, are shown. The same quantities are shown for the outer parts of Abell 2390 and Coma for comparison. (See Abraham et al. (1996) for more detail on the latter.)

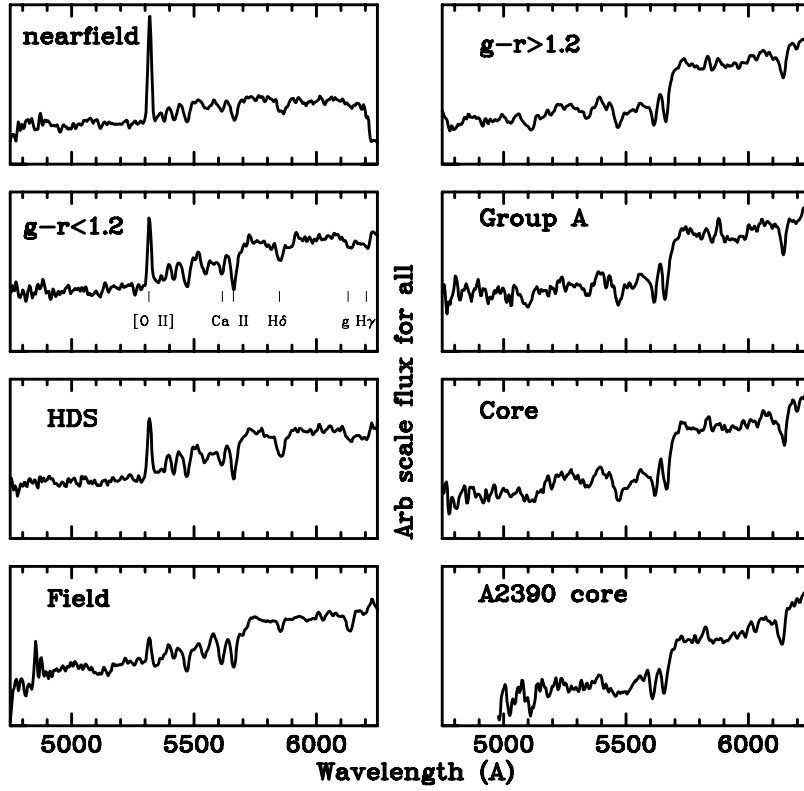


Fig. 8.— Co-added spectra from subsets of galaxies, in the observed wavelength frame. For comparison, the average of the central galaxies of Abell 2390 are shown shifted to the redshift of MS1621.5+2640. Fluxes are arbitrarily scaled for easy comparison.

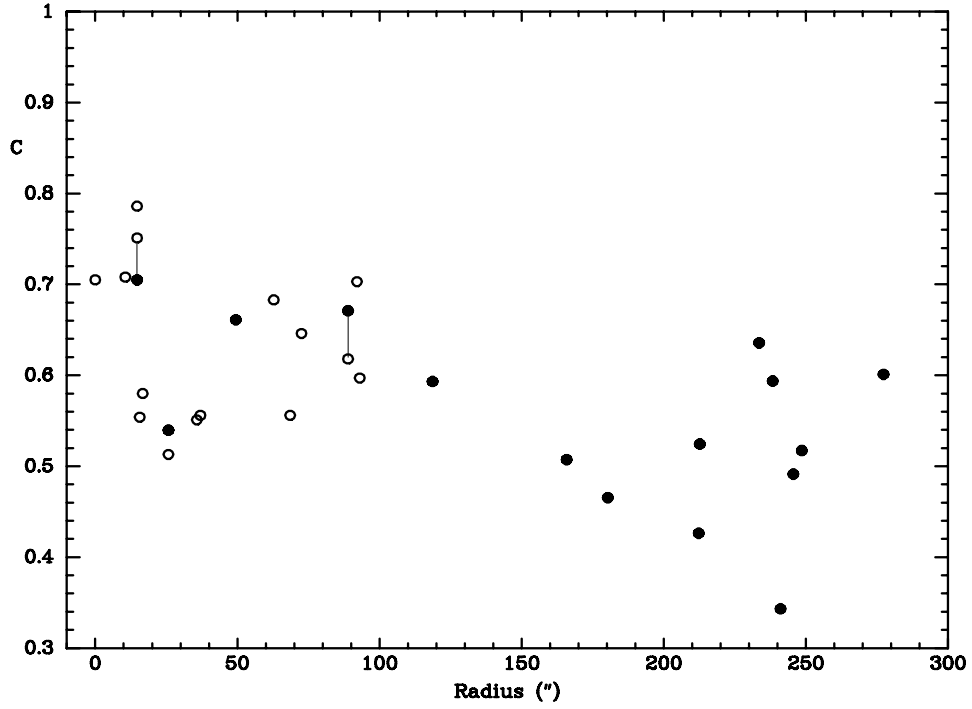


Fig. 9.— Galaxy central concentration for cluster members with projected radius. The open points are from SIS image and the filled points from MOS data. The zero-points are adjusted to minimize the differences in values for the two galaxies in common, whose symbols are connected.

Fig. 10.— (Removed due to problems with LANL policy on file sizes. Can be obtained from: <http://www.hia.nrc.ca/STAFF/slm/ms1621>) ROSAT HRI map with the locations of the galaxies with measured redshifts in the CNOC sample overlaid. Circles indicate cluster members, while plusses mark the positions of fore and background galaxies with redshifts. ‘Near-field’ galaxies are marked as crosses. Black on the grayscale corresponds to an HRI detection rate of roughly 3×10^{-6} counts s^{-1} arcsec^{-2} . The region plotted is slightly larger than the spectroscopically surveyed field of 9 arcmin by 23.3 arcmin.

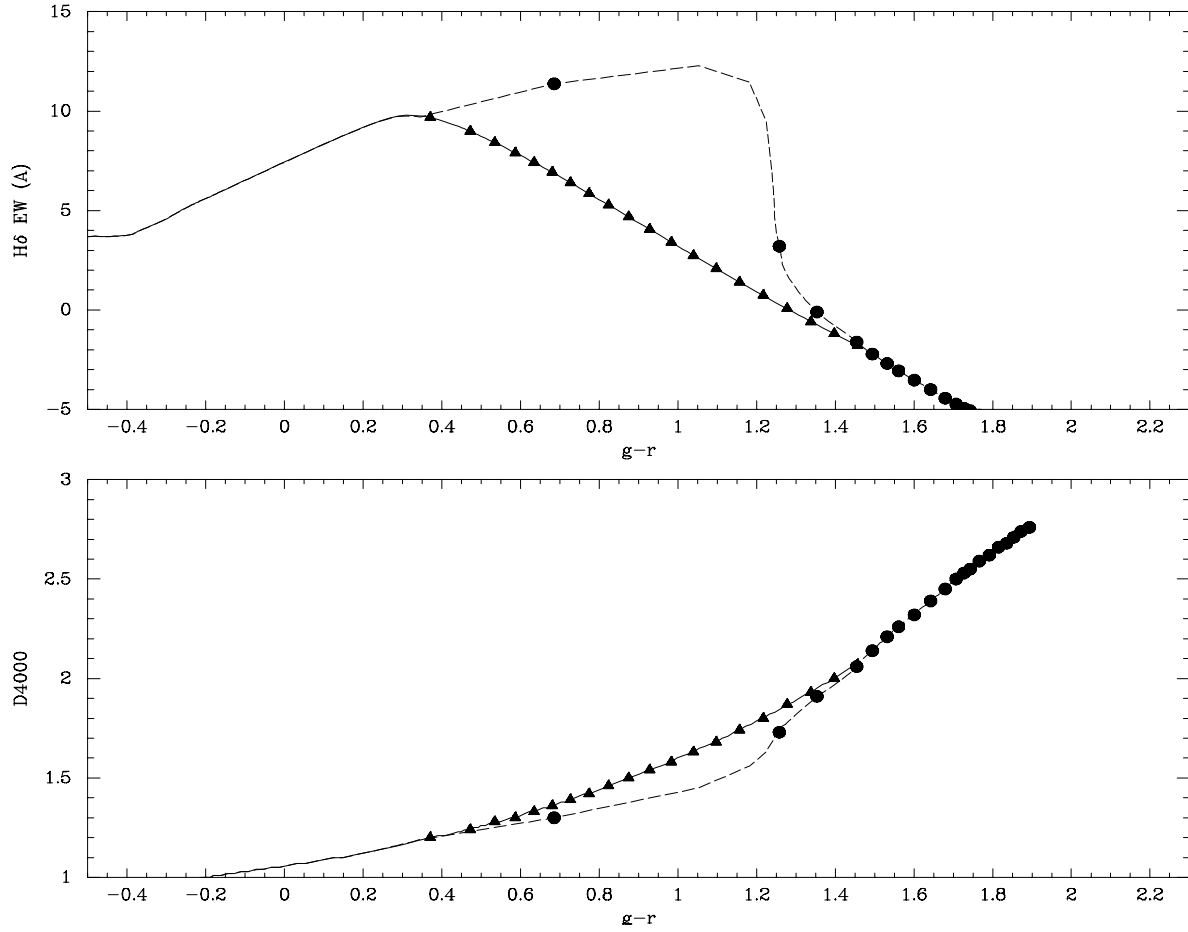


Fig. 11.— GISSSEL96 models (Bruzual & Charlot (1993)) with Salpeter IMF and solar metallicity, for redshift 0.4274. The dashed line shows a track for 1 Gyr of continuous star formation followed by complete cessation. The solid line shows exponentially decreasing star-formation with a time constant 4 Gyr. Symbols indicate ages at 1 Gyr intervals from 1 to 20 Gyr.

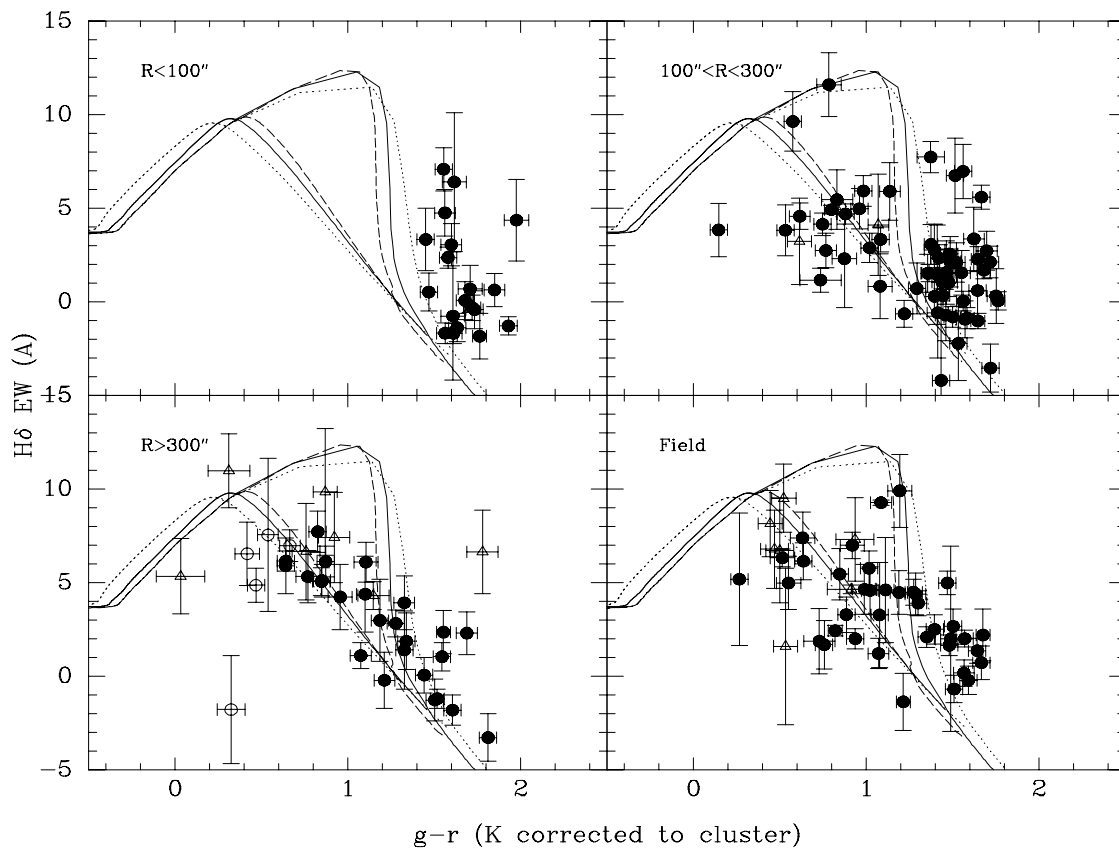


Fig. 12.— $H\delta$ versus $g-r$ color for 3 projected radius bins in the cluster and for the field (k-corrected to the cluster redshift). Open triangles are member galaxies with r magnitude fainter than 22.0 (see § 3), open circles are the near-field galaxies. The lines sketch the models illustrated more clearly in Figure 11. The solid line shows solar metallicity, the dashed line is 0.4 times solar, and the dotted line is 2.5 times solar.

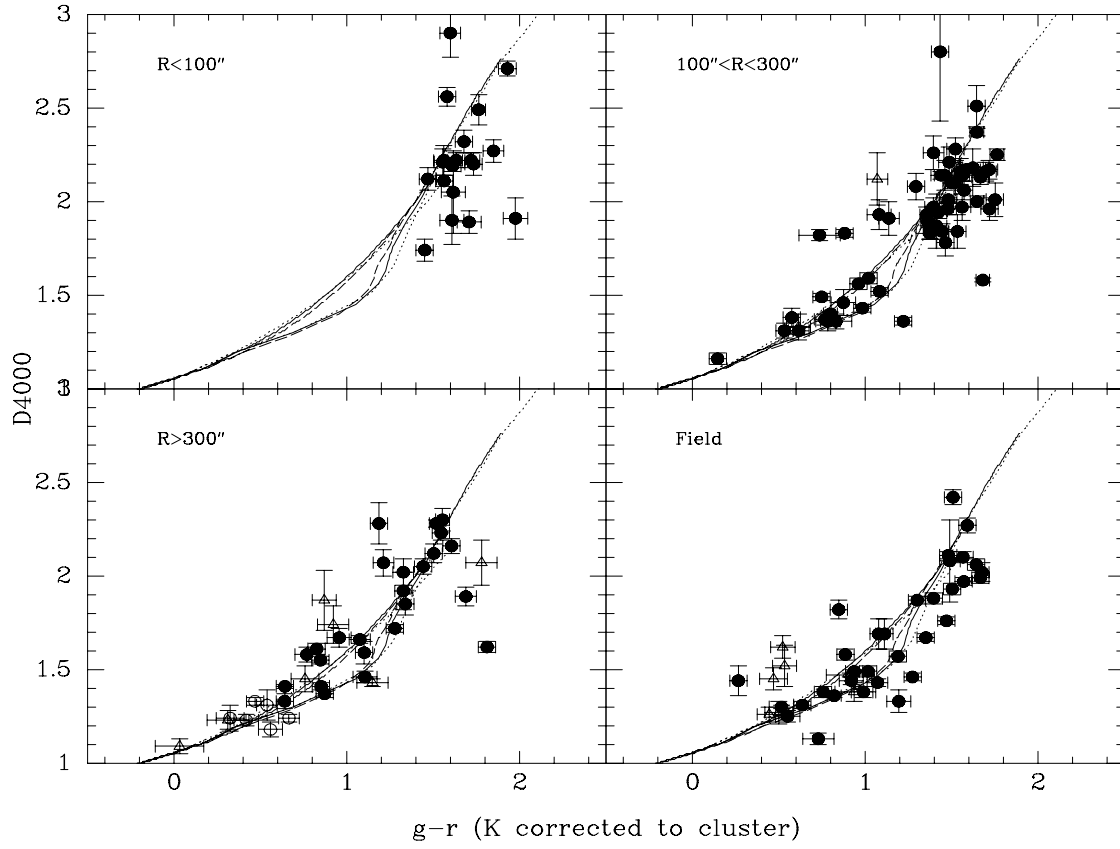


Fig. 13.— As Figure 12 but for D4000.

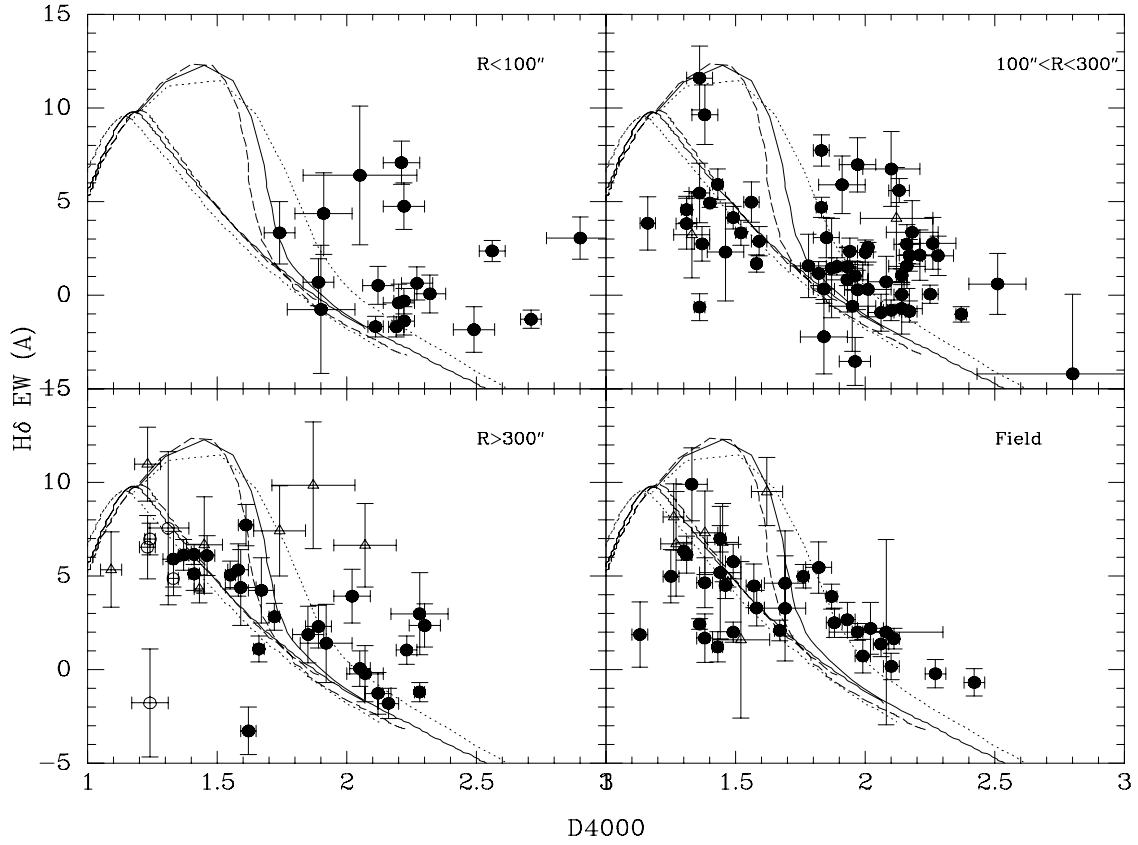


Fig. 14.— As Figure 12 but plotting the two spectroscopic measures to avoid reddening uncertainty.

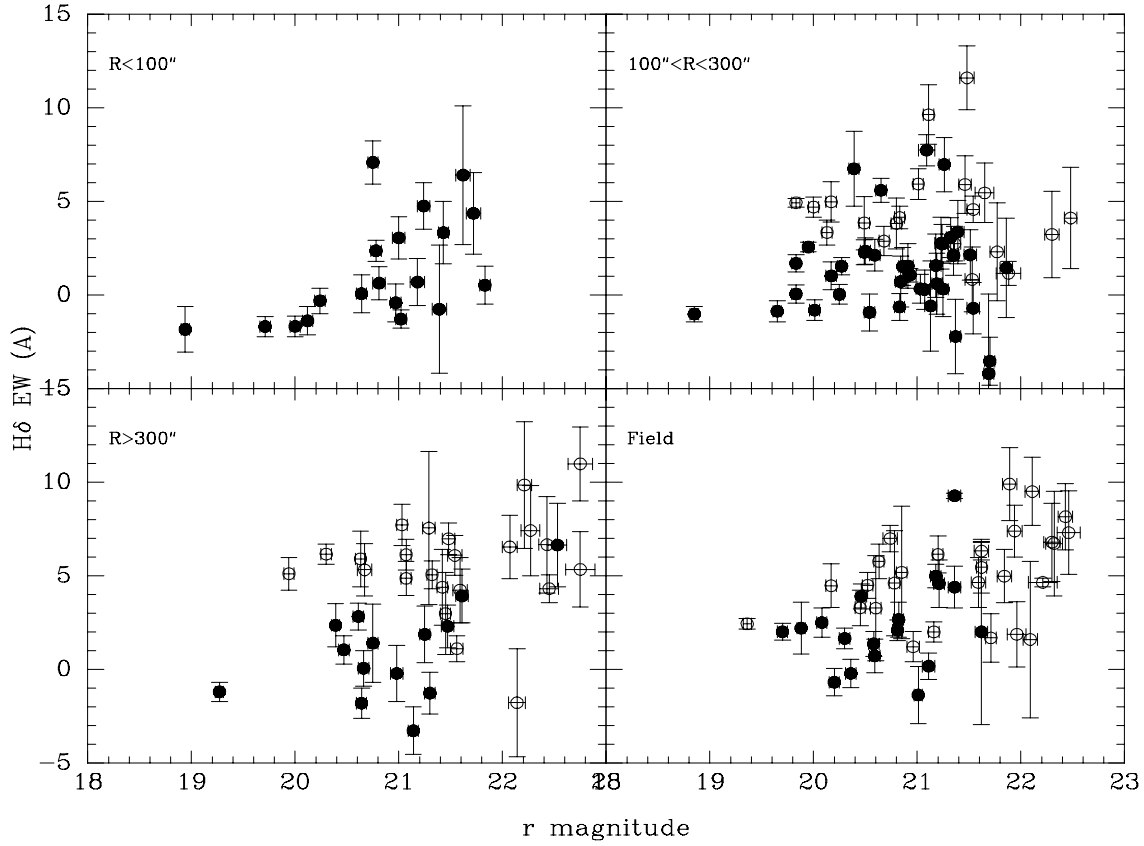


Fig. 15.— $H\delta$ versus apparent r magnitude. As all the objects in the cluster (and indeed the field sample) are at roughly the same redshift, this is proportional to luminosity. Filled symbols are galaxies with $g-r$ color ≥ 1.2 (red), while open symbols are galaxies with $g-r$ color < 1.2 (blue). See § 3 for a discussion of the unbiased magnitude range.

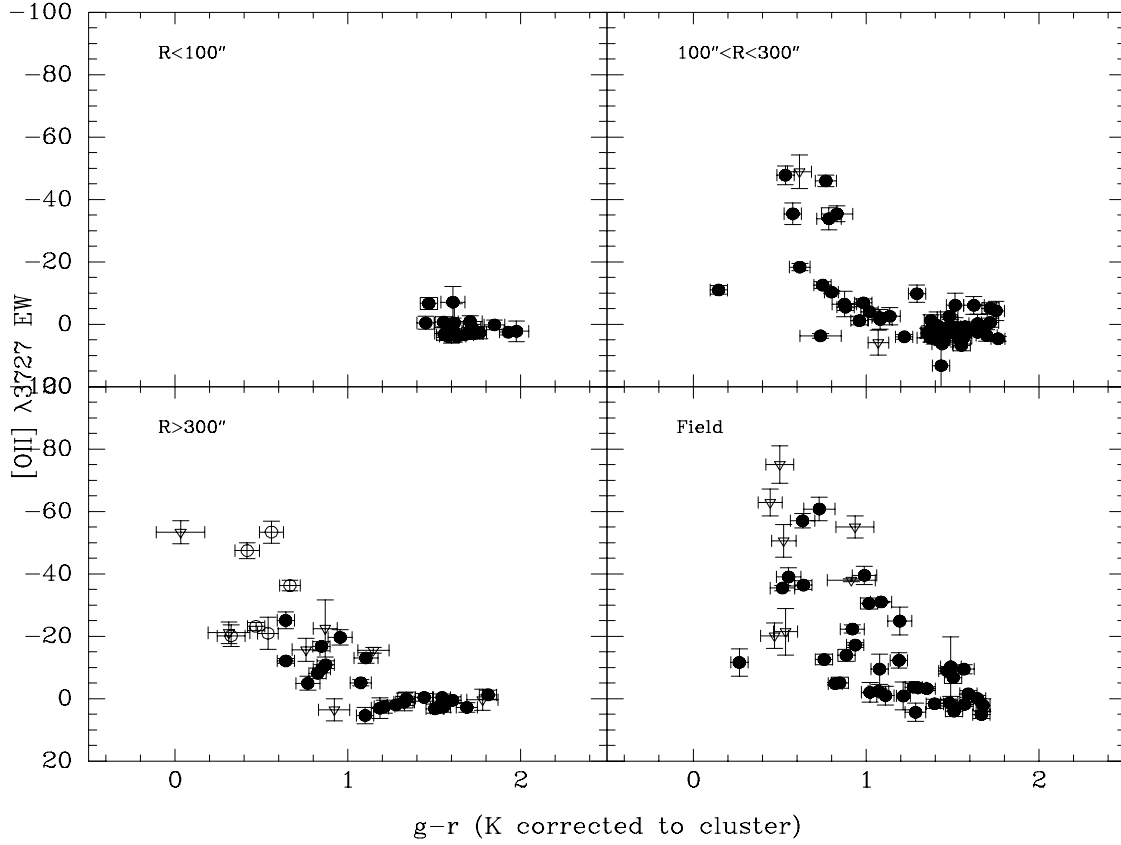


Fig. 16.— As Figure 12 for [O II] emission. The GISEL models (Bruzual & Charlot (1993)) do not include emission lines, and hence no model lines are plotted.

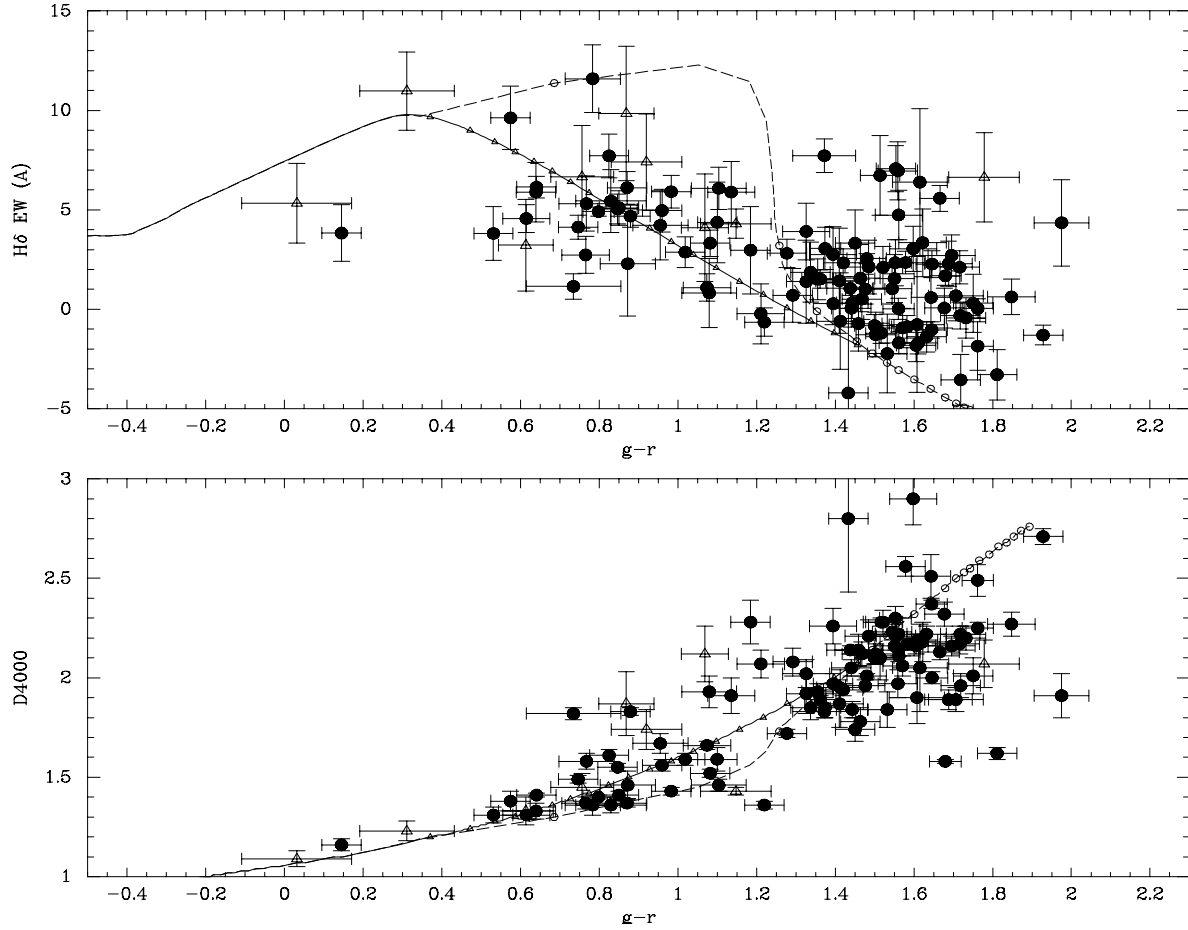


Fig. 17.— Measured quantities for all cluster members (i.e. summing over all radii) compared with solar metallicity models from Figure 11. Open triangles are member galaxies with r magnitude fainter than 22.0 (see § 3).

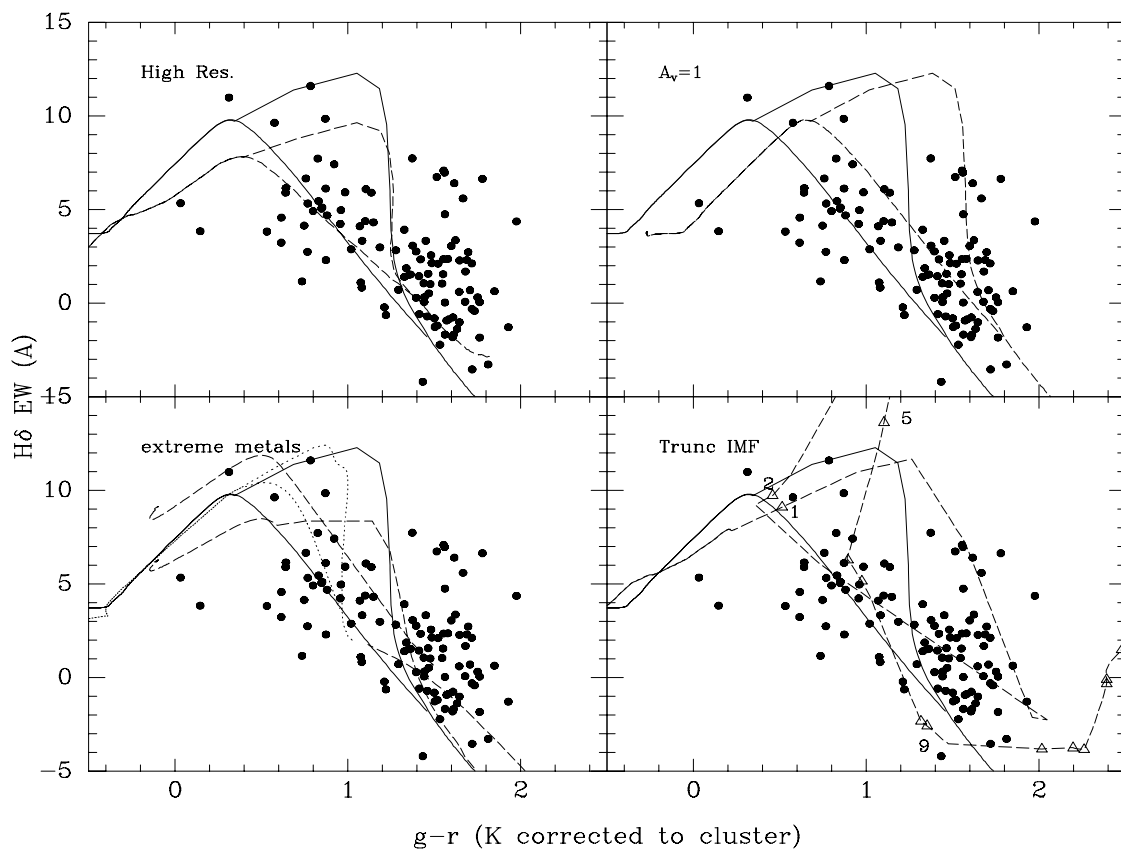


Fig. 18.— As Figure 17 with the solar metallicity standard models plotted as solid lines, but also with model lines plotted for: (top-left) a Bruzual and Charlot solar metallicity model from 1995 with much higher spectral resolution, (top-right) the standard model shifted for a reddening $A_v=1$ ($E(g-r)=0.3312$), (bottom-left) 5 times solar metallicity (dashed line), and 1/50 times solar metallicity (dotted line), and (bottom-right) Bruzual and Charlot solar metallicity model from 1995 with an IMF with no stars of mass less than 2.5 times solar. A few times (in Gyr) have been marked on the model line. For clarity, the error bars have been removed from the data points. The error bars can be seen in Figure 12.

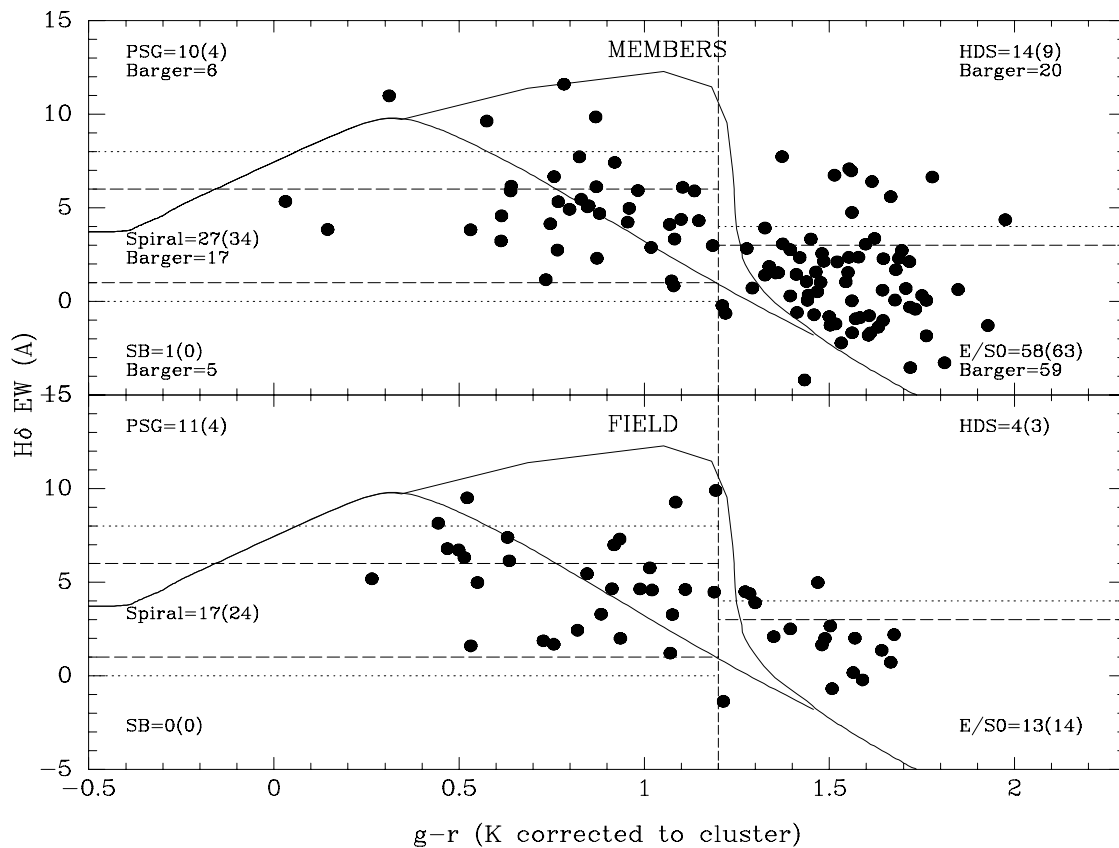


Fig. 19.— As Figure 17 with the solar metallicity standard models plotted as solid lines, but also with the dividing lines proposed by Barger et al. (1996) shown as dashed lines, and some alternative dividing lines proposed in this paper shown as dotted lines. Top panel shows cluster members, bottom panel shows the field sample for the same redshift. See the text for explanation of the numbers listed. For clarity, the error bars have been removed from the data points. The error bars can be seen in Figure 12 and 13.

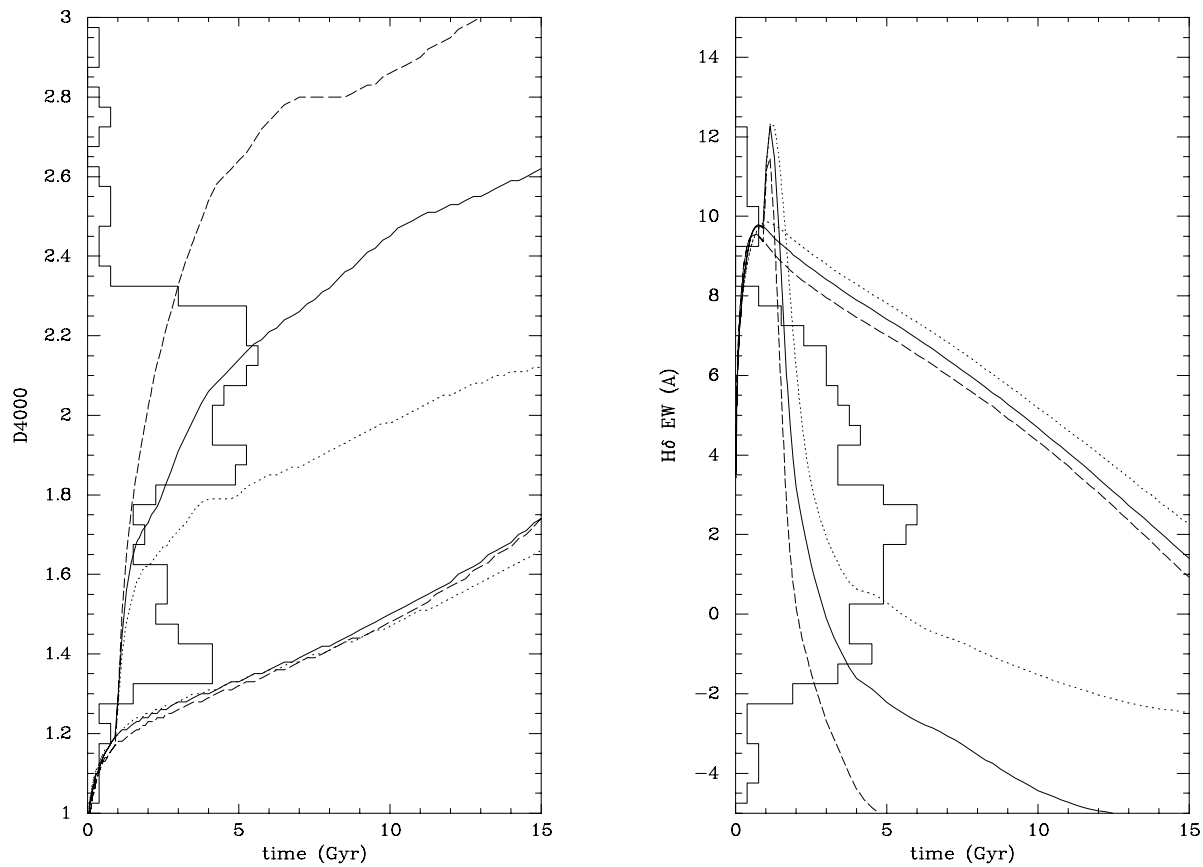


Fig. 20.— Age/Metallicity measures of the oldest galaxies. Left panel shows model curves of D4000 versus age from solar (solid), 2.5 times solar (dashed) and 0.4 times solar (dotted) metallicity models. The upper curves are for a 1 Gyr burst of star formation (ellipticals), while the lower curves are for exponentially falling star formation with a time constant of 4 Gyrs (spirals). Also plotted is the histogram of observed D4000 for cluster members. The Right panel shows the same curves and data but for H δ rather than D4000. The ‘spiral’ curves in this case lie above the ‘elliptical’ curves for times later than 3 Gyrs.